EGFP-expressing populations. (B) hADMPCs transduced with CSII-CMV-EGFP or CSII-EF-EGFP at m.o.i. of 100, 250, 500, and 1000 were analyzed. (C) hADMPCs transduced with CSII-CMV-EGFP or CSII-EF-EGFP at m.o.i. of 1000 were analyzed over a 28 day period. Error bars represent the standard error of 3 independent analyses. **, $P<0.01$; *, $P<0.05$ (Student's t test).
doi:10.1371/journal.pone.0066274.g001

100, 250, 500, and 1000. Four days later, the cells were analyzed with a Guava easyCyte 8HT flow cytometer (Merck-Millipore) using an argon laser at 488 nm. Dead cells were excluded with the LIVE/DEAD fixable far red dead cell stain kit (Invitrogen). For analysis of hADMPCs transduced with pTRE-EGFP-EF-tTA-2A-Bsd or pTRE-EGFP-CMV-tTA-2A-Bsd, hADMPCs were transduced with the lentiviral vector at a m.o.i. of 250 and were cultured with or without 1 μg/mL Dox. Four days later, a part of the cells were analyzed with a Guava easyCyte 8HT flow cytometer. The rest of the cells were cultured with 4 μg/mL blasticidin and 1 μg/mL Dox for 3 weeks. Then, the cells were seeded in 6-well plates and cultured with or without Dox for 4 days. The cells were harvested and re-suspended in staining buffer (PBS containing 1% BSA, 2 mM EDTA, and 0.01% sodium azide) at a density of 1×10^6 cells/mL and incubated with phycoerythrin (PE)-conjugated antibody against CD13, CD29, CD34, CD44, CD73, CD90, CD105, or CD166 for 20 min. Non-specific staining was assessed using relevant isotype controls. 525/30 nm and 583/26 nm band pass filters were used for the detection of EGFP and PE, respectively. Dead cells were excluded with the LIVE/DEAD fixable far red dead cell stain kit (Invitrogen). FlowJo software (TreeStar Inc., Ashland, OR, USA) was used for quantitation analysis. The threshold for gating was determined as the fluorescence value above which less than 1% of the control cells were considered as positive events.

Fluorescence Microscopy

Phase contrast and fluorescence images were obtained using Fluorescence Microscope (BZ-9000; Keyence, Osaka, Japan) using BZ Analyzer Software (Keyence).

Adipogenic, Osteogenic, Chondrogenic, and Neurogenic Differentiation Procedures

For adipogenic differentiation, cells were cultured in differentiation medium (Zen-Bio, Durham, NC, USA). After 3 days, half of the medium was changed to adipocyte medium (Zen-Bio), and this was repeated every 3 days. Three weeks after differentiation, characterization of adipocytes was confirmed by microscopic observation of intracellular lipid droplets by oil red O staining. Osteogenic differentiation was induced by culturing the cells in DMEM containing 10 nM dexamethasone, 50 mg/dL ascorbic acid 2-phosphate, 10 mM β-glycerophosphate (Sigma), and 10% FBS. Differentiation was examined by alizarin red staining. For chondrogenic differentiation, 2×10^5 hADMPCs were centrifuged at 400× *g* for 10 min. The resulting pellets were cultured in chondrogenic medium (α-MEM supplemented with 10 ng/mL transforming growth factor-β, 10 nM dexamethasone, 100 mM ascorbate, and 1× insulin–transferrin–selenium solution) for 14 days, as described previously [27]. The pellets were fixed with 4% paraformaldehyde in PBS, embedded in OCT, frozen, and sectioned at 8 μm. The sections were incubated with PBSMT (PBS containing 0.1% Triton X-100, 2% skim milk) for 1 h at room temperature, and then incubated with mouse monoclonal antibody against type II collagen (Abcam, Cambridge, MA, USA) and rabbit polyclonal antibody against GFP (Invitrogen) for 1 h. After washing with PBS, cells were incubated with Alexa 546 conjugated anti-mouse IgG and Alexa 488 conjugated anti-rabbit IgG for chondrocytes (Invitrogen) or Alexa 546 conjugated anti-rabbit IgG and Alexa 488 conjugated anti-rat IgG (Invitrogen) for neuronal cells. The cells were counterstained with 4′-6-diamidino-2-phenylindole (DAPI) (Invitrogen) to identify cellular nuclei. For neurogenic differentiation, cells were cultured in Hyclone AdvanceSTEM neural differentiation medium (Thermo Scientific, South Logan, UT, USA) for 2 days. Differentiation was examined by immunofluorescent staining against β3-tubulin. Cells were fixed with 4% paraformaldehyde in PBS for 10 min at 4°C and then washed 3 times in PBS. Blocking was performed with PBSMT for 1 h at room temperature. The differentiated cells were incubated with rabbit monoclonal antibody against β3-tubulin (Cell Signaling Technologies, Danvers, MA, USA) and rat monoclonal antibody against GFP (Nacalai, Kyoto, Japan). After washing with PBS, cells were incubated with Alexa 546 conjugated anti-rabbit IgG and Alexa 488 conjugated anti-rat IgG (Invitrogen). The cells were counterstained with 4′-6-diamidino-2-phenylindole (DAPI) (Invitrogen) to identify cellular nuclei.

Results

The Efficiency of the EF-1α Promoter was Higher than that of the CMV Promoter in hADMPCs

To determine the efficiency of the EF-1α promoter and the CMV promoter, hADMPCs were transduced with CSII-EF-EGFP or CSII-CMV-EGFP at a m.o.i. of 25, 50, 100, 250, 500, and 1000 and analyzed by flow cytometry. As shown in Figure 1A, percentage of GFP-positive cells increased in a dose-dependent manner. Intriguingly, transduction efficiency of CSII-EF-EGFP was significantly higher than that of CSII-CMV-EGFP in hADMPCs (Figure 1A). Moreover, a higher induction level of GFP was observed under the EF-1α promoter than under the CMV promoter, based on the median fluorescent intensity (Figure 1B). Furthermore, GFP fluorescent intensities driven from the CMV promoter were significantly decreased (from 100% on day 7 to 49.3% on day 21 and 38.4% on day 28; Figure 1C), indicating that promoter silencing occurred as previously reported [19]. In contrast, hADMPCs transduced with CSII-EF-EGFP sustained GFP expression levels with no significant reduction throughout the 28-day experimental period (Figure 1C).

Construction and Characterization of Dual-promoter Lentiviral Vectors in hADMPCs

Next, we constructed dual-promoter lentiviral vectors, which contain TRE-Tight followed by an improved version of tet-controlled transactivator (tTA advanced) induced under the CMV or EF-1α promoter (Figure 2A). In this "single tet-off lentiviral vector platform", the regulator and response elements are combined in a single lentiviral genome, along with a Gateway cassette containing *att*R recombination sites flanking a *ccd*B gene and a chloramphenicol-resistance gene, which allows an easy and rapid shuttling of the gene of interest into the vectors using the Gateway LR recombination reaction (Figure 2A). Using this system, we constructed pTRE-EGFP-CMV-tTA-2A-Bsd or pTRE-EGFP-EF-tTA-2A-Bsd (Figure 2B). Both the CMV and the EF-1α promoters drive the mRNA expression of tTA advanced linked to the Bsd gene by the Thosea asigna virus 2A (T2A) peptide sequence. This single transcript is then translated and cleaved into 2 proteins; tTA advanced carrying 2A tag at the

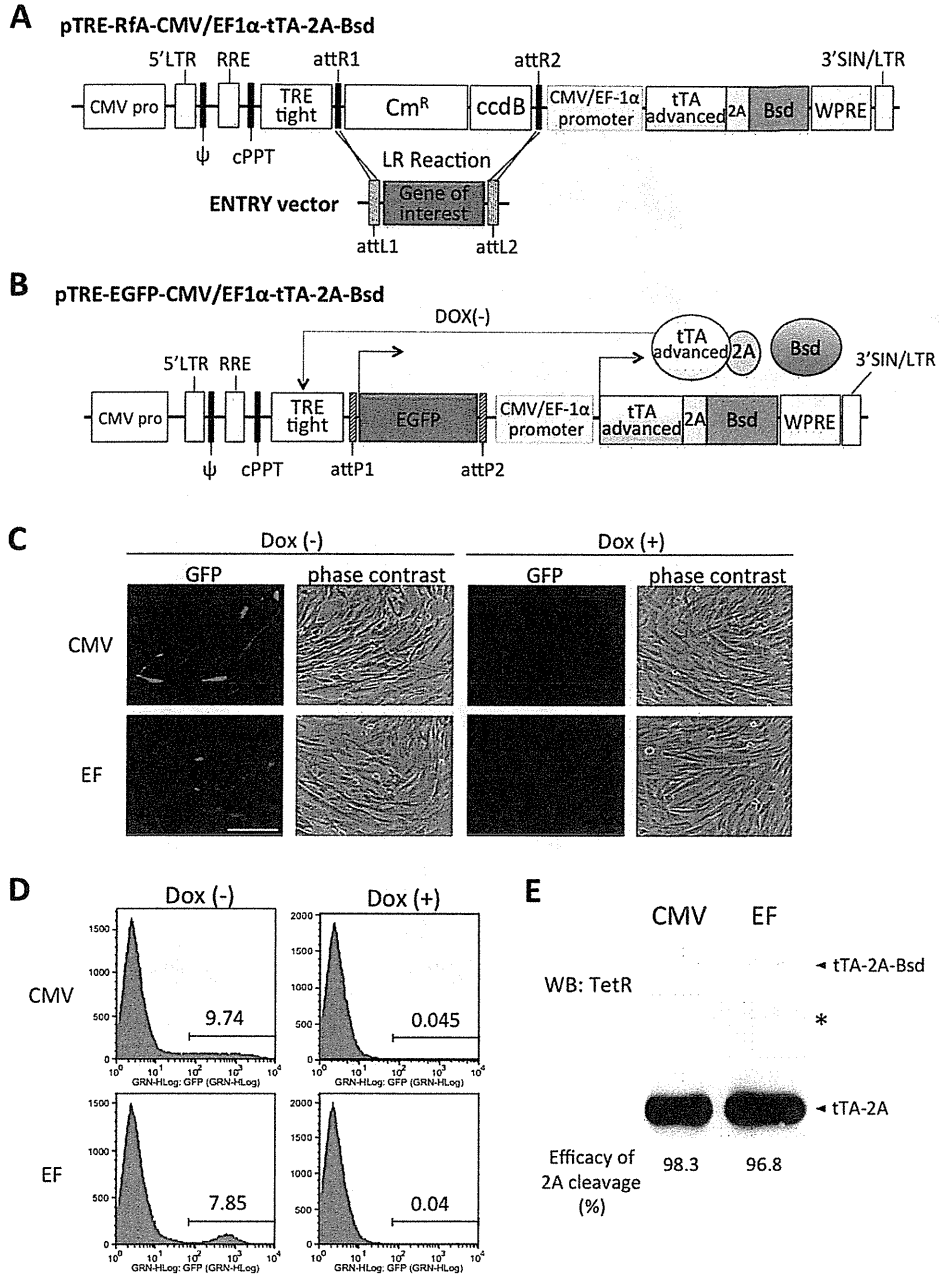

Figure 2. Schematic drawings of the single lentiviral vectors for tet-off system used in this work. (A) Gateway-compatible destination vectors containing *att*R recombination sites flanking a *ccd*B gene and a chloramphenicol-resistance gene, which allows an easy and rapid shuttling of gene of interest flanked by attL sites into the destination vectors using the Gateway LR recombination reaction. They also have an improved version of tetracycline-controlled transactivator (tTA) linked to the blasticidin resistant (Bsd) gene by the Thosea asigna virus 2A (2A) peptide sequence, whose expression is regulated by the CMV or EF-1α promoter. In the present study, we constructed an entry vector encoding EGFP flanked by attL, resulting in a destination clone, pTRE-EGFP-CMV-tTA-2A-Bsd or pTRE-EGFP-EF-tTA-2A-Bsd (B). In the absence of doxycycline (Dox), tTA-2A binds to the TRE-Tight promoter and activates EGFP transcription. For more details, see the Results section. CMV pro, CMV promoter; LTR, long terminal repeats; ψ, packaging signal; RRE, rev response elements; cPPT, central polypurine tract; TRE, tet-responsive element; Cm^R, chloramphenicol resistance; tTA, tetracycline-controlled transactivator; Bsd, blasticidin resistance; WPRE, woodchuck hepatitis virus posttranscriptional control element; SIN, self-inactivating. (C) (D) hADMPCs were transduced with pTRE-EGFP-CMV-tTA-2A-Bsd or pTRE-EGFP-EF-tTA-2A-Bsd at m.o.i. of 250. Four days after transduction, the cells were divided into 2 populations; with 1 μg/mL of Dox (Dox (+)) and without Dox (Dox (-)). (C) Fluorescent and phase contrast images. Scale bar, 200 μm. (D) Log fluorescence histograms of EGFP by flow cytometry analysis. (E) The whole cell lysates from hADMPCs transduced with pTRE-EGFP-CMV-tTA-2A-Bsd or pTRE-EGFP-EF-tTA-2A-Bsd were subjected to western blotting to monitor the cleavage efficiency of tTA-2A-Bsd proteins. A primary antibody against TetR was used to detect either tTA-2A-Bsd (non-cleaved form) or tTA-2A (cleaved form). Asterisk indicates a nonspecific band.

doi:10.1371/journal.pone.0066274.g002

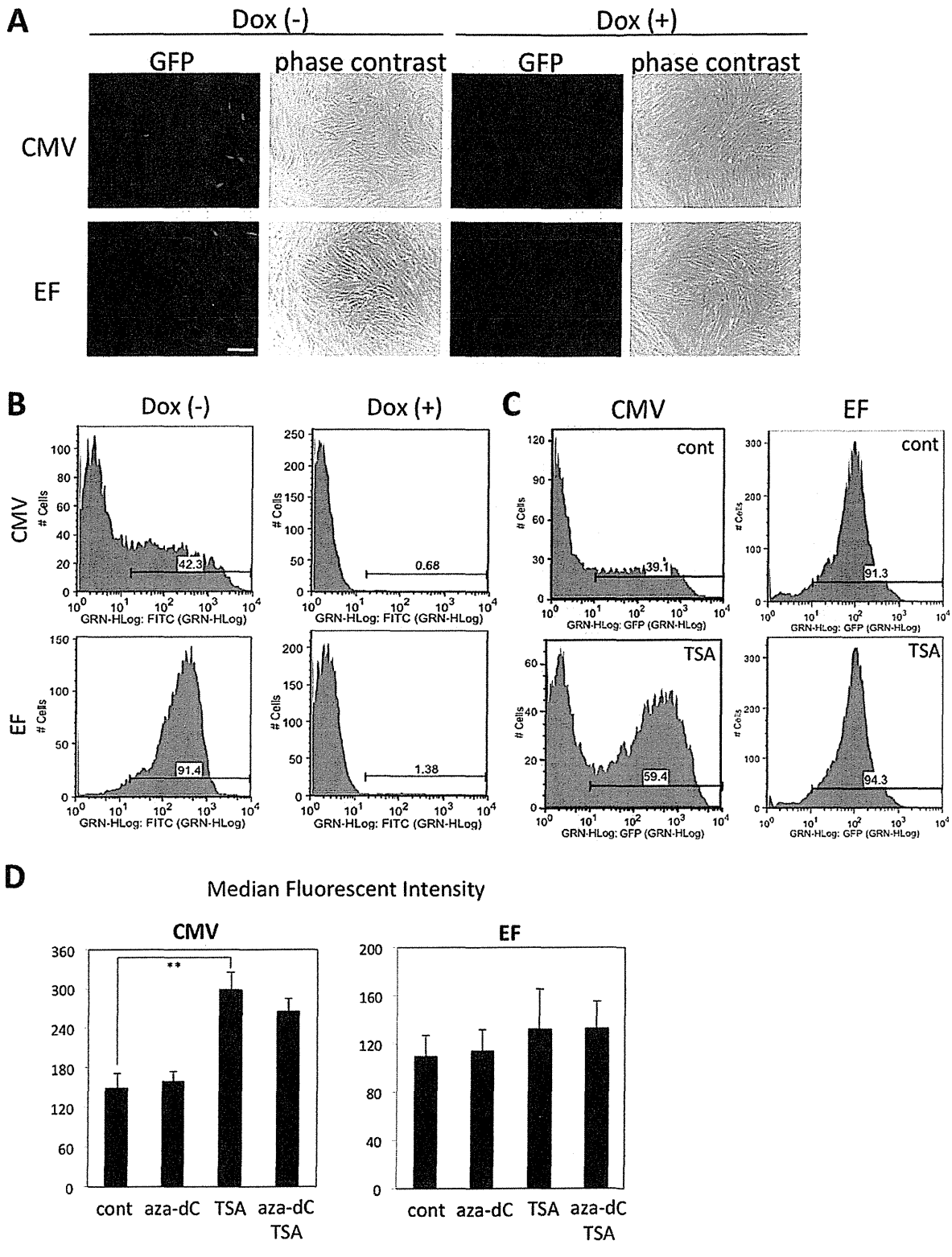

Figure 3. Blasticidin selection of hADMPCs transduced with single tet-off lentiviral vector platform. hADMPCs were transduced with pTRE-EGFP-CMV-tTA-2A-Bsd (CMV) or pTRE-EGFP-EF-tTA-2A-Bsd (EF) at m.o.i. of 250. The cells were treated with 4 μg/mL blasticidin and 1 μg/mL Dox for 2 weeks. Then, the cells were cultured in the absence (Dox (-)) or presence (Dox (+)) of 1 μg/mL Dox for 4 days, and analyzed under a microscope (A) and flow cytometer (B). The cells were treated with 100 nM TSA (TSA), 5 μM 5-aza-dC (aza-dC), or both for 48 h before analyzed by flow

cytometer. (C) A representative fluorescence histogram of EGFP. (D) The median fluorescence intensities of the EGFP-expressing populations. Error bars represent the standard error of 3 independent analyses. **, $P<0.01$ (Student's t test). Scale bar, 200 μm.
doi:10.1371/journal.pone.0066274.g003

C-terminus (tTA-2A) and Bsd. tTA-2A binds to the TRE-tight in the absence of Dox, a tet derivative, and activates transcription of EGFP to a very high level. In the presence of Dox, tTA-2A is unable to bind the TRE-Tight in a tet-responsive promoter, and the system is inactive.

To investigate the usefulness of these lentiviral vectors, hADMPCs were transduced with pTRE-EGFP-CMV-tTA-2A-Bsd or pTRE-EGFP-EF-tTA-2A-Bsd at a m.o.i. of 250. As shown in Figure 2C, expression of EGFP was observed in the absence of Dox, whereas addition of Dox (1 μg/mL) was enough to suppress the expression. Flow cytometry analysis revealed that the transduction efficiency was relatively low (EGFP-positive cells were 7.5~10%) compared with that of CSII-CMV-EGFP or CSII-EF-EGFP (EGFP-positive cells were 45% or 77% at a m.o.i. of 250, respectively; Figure 1A), and the tet-off system completely abolished gene expression in the presence of Dox (Figure 2D). Flow cytometry analysis also revealed that fluorescent intensity was relatively uniform in hADMPCs transduced with pTRE-EGFP-EF-tTA-2A-Bsd, but a wide range of fluorescent intensities was observed in hADMPCs infected with pTRE-EGFP-CMV-tTA-2A-Bsd. These data suggest that tTA-2A functions properly in this system. Moreover, western blot analysis against tTA showed the efficient cleavage (>95%) of tTA-2A-Bsd proteins into tTA-2A and Bsd (Figure 2E).

To further determine that Bsd cleaved from tTA-2A-Bsd was effective in this system, 4 μg/mL blasticidin was administered to hADMPCs. Within 1 week after the selection, control hADMPCs were completely killed (data not shown), whereas hADMPCs that were successfully transduced with either pTRE-EGFP-CMV-tTA-2A-Bsd or pTRE-EGFP-EF-tTA-2A-Bsd could survive and proliferate, demonstrating that Bsd from tTA-2A-Bsd is sufficient to confer blasticidin resistance to the cells. The surviving cells were kept in culture medium with blasticidin and then divided into 2 populations, either with Dox (1 μg/mL) or without Dox. As shown in Figure 3A and 3B, almost all (>90%) the cells transduced with pTRE-EGFP-EF-tTA-2A-Bsd strongly expressed EGFP in the absence of Dox. In hADMPCs transduced with pTRE-EGFP-CMV-tTA-2A-Bsd, however, >50% of the cells were EGFP negative regardless of their blasticidin resistance. Moreover, fluorescent intensities were quite variable; some cells expressed very high levels of EGFP, while others expressed very low levels (Figure 3A and 3B). This might be due to "promoter suppression," transcript repression of an upstream transcriptional unit by a downstream unit when 2 transcriptional units lie adjacent in head-to-tail tandem on a chromosome [28,29]. Studies have revealed that the suppression by adjacent units is epigenetic and involves modification of the chromatin structure, including DNA methylation at CpG sites within the promoter, histone deacetylation, histone methylation at specific residues (e.g., H3K9, H3K27), and densely packed nucleosomes that create a closed chromatin structure. In order to determine if inhibiting histone deacetylases or DNA methylation would re-induce EGFP expression, pTRE-EGFP-CMV-tTA-2A-Bsd cells were treated with histone deacetylase inhibitor trichostatin A (TSA) and/or DNA methylation inhibitor 5-aza-2′-deoxycytidine (5-aza-dC). TSA treatment significantly increased the number of EGFP-positive cells and strengthened the fluorescent intensities of EGFP, whereas 5-aza-dC had no effect, suggesting that EGFP expression was repressed by histone deacetylation when stably transduced with pTRE-EGFP-CMV-tTA-2A-Bsd (Figure 3C and 3D). These inhibitors had no effect on hADMPCs transduced with pTRE-EGFP-EF-tTA-2A-Bsd. These data suggest that the dual-promoter lentiviral vector using the EF promoter is more resistant to gene silencing than that using the CMV promoter.

Blasticidin-selected hADMPCs Maintain the Properties of Their Parental hADMPCs

hADMPCs are an attractive material for cell therapy because of their ability to secrete various cytokines and growth factors. These cells also have the ability to differentiate into various types of cells, including adipocytes, chondrocytes, osteocytes, hepatocytes, cardiomyoblasts, and neuronal cells. Gene manipulation of hADMPCs may thus generate great possibilities for cell therapy and tissue engineering. From this point of view, the development of an efficient and stable Dox-responsive gene transfer system to achieve high levels of transgene expression in hADMPCs, without affecting the phenotype, is of special interest for the field. We therefore studied the cell properties of hADMPCs transduced with the single tet-off lentiviral vector after blasticidin selection. Flow cytometry analysis revealed no changes in the expression of the main surface markers (positive for CD13, CD29, CD44, CD73, CD90, CD105, and CD166, and negative for CD34) either in the absence or presence of Dox (Figure 4). To further confirm the properties of hADMPCs, the cells were differentiated into adipocytes, osteocytes, chondrocytes, and neuronal cells. As shown in Figure 5, blasticidin-selected hADMPCs maintained their ability to differentiate into adipocytes, osteocytes, chondrocytes, and neuronal cells. Moreover, EGFP was stably expressed in the differentiated cells only in the absence of Dox (Figure 5).

Discussion

In recent years, there is growing interest in the use of MSCs for cell therapy and tissue engineering because of their differentiation potential and ability to secrete growth factors [7–11]. Furthermore, because of their hypo-immunogenicity and immune modulatory effects, MSCs are good candidates for gene delivery vehicles for therapeutic purposes [12,14]. In addition to primary MSCs, genetically modified MSCs have been applied to bone regeneration, muscle repair, diabetes, Parkinson's disease, and myocardial infarction recovery [14,30–35]. Duan et al. reported that the angiogenic effect of MSCs could be enhanced by adenovirus-mediated HGF overexpression in the treatment of cardiac ischemia injury [14]. Karnieli et al. and Li et al. both reported the reversal of hyperglycemia in streptozotocin-induced diabetic mice after transplantation of insulin-producing cells originating from genetically modified Pdx-1 expressing MSCs [32,33].

While significant progress has been made in the use of genetically modified MSCs for basic and applied research, the current methods for gene manipulation are still insufficient for some applications. Adenoviral vectors are commonly used for transient expression because they remain epichromosomal in the host cells, and their ability to transiently infect target cells minimizes the risk of insertional mutagenesis [36]. However, relatively brief transgene expression may limit the utility of this approach to tissue repair applications. On the other hand, lentiviral vectors, which are promising vectors for gene delivery in primary human cells, integrate into the host cell genome, which may be an appropriate strategy for tissue repair applications

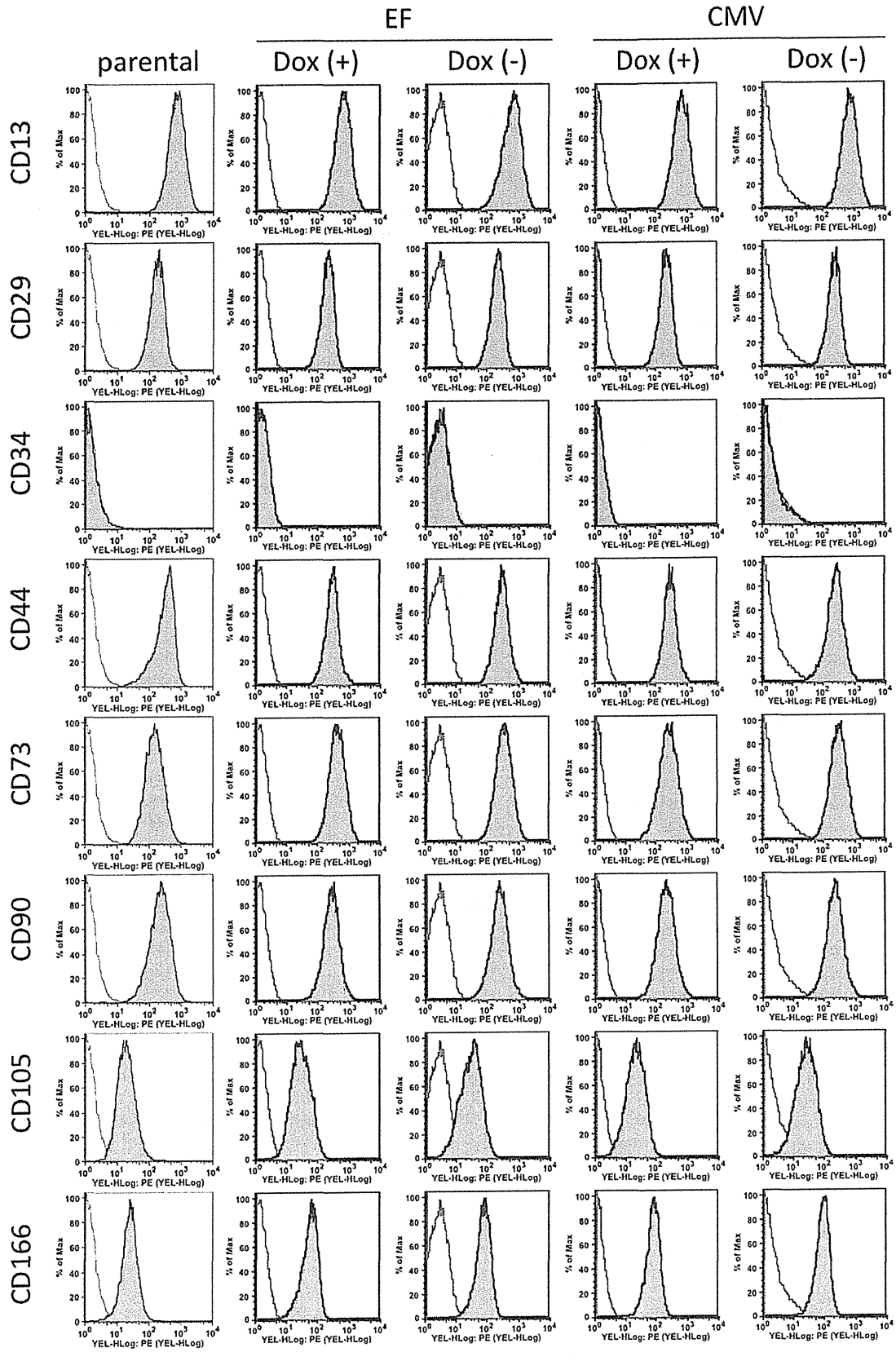
EF
CMV
parental
Dox (+)
Dox (-)
Dox (+)
Dox (-)
CD13
CD29
CD34
CD44
CD73
CD90
CD105
CD166
% of Max
YEL-HLog: PE (YEL-HLog)

Figure 4. Expression pattern of surface cell markers on Dox-responsive hADMPCs. Dox-responsive hADMPCs after selection by blasticidin were cultured in the absence (Dox(-)) or presence (Dox (+)) of 1 μg/mL Dox for 4 days. Expression of the different surface markers were analyzed by flow cytometry and compared to the expression by a parental hADMPCs. They were stained with PE-coupled antibodies against CD13, CD29, CD34, CD44, CD73, CD90, CD105, and CD166. Histogram of a PE-coupled mouse IgG1 κ isotype control is shown in gray. CMV; hADMPCs transduced with pTRE-EGFP-CMV-tTA-2A-Bsd, EF; hADMPCs transduced with pTRE-EGFP-EF-tTA-2A-Bsd.
doi:10.1371/journal.pone.0066274.g004

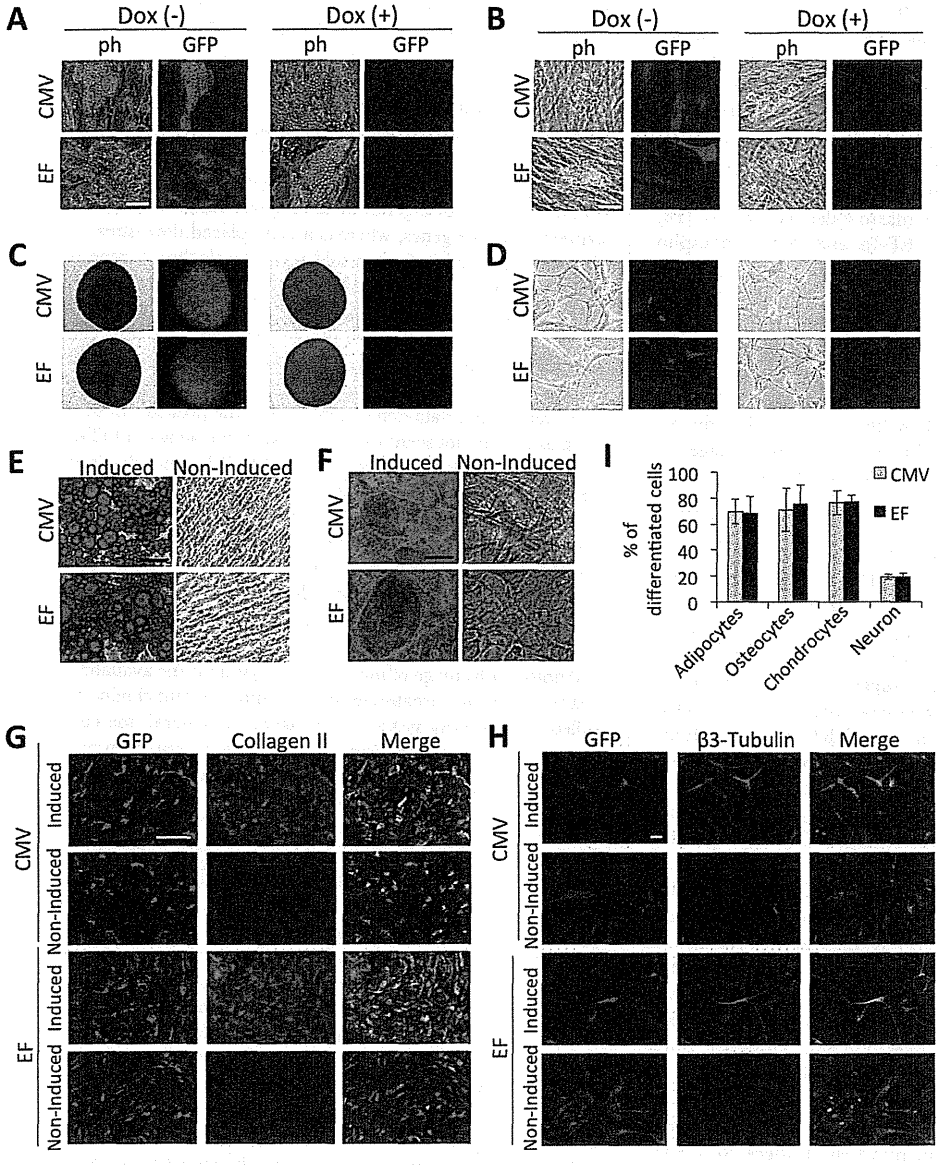

Figure 5. Differentiation potential of Dox-responsive hADMPCs. *Dox-responsive hADMPCs were differentiated into adipocytes (A, E), osteocytes (B, F), chondrocytes (C, G), and neuronal cells (D, H). (A–D) Phase contrast (ph) and fluorescent (GFP) images. Dox-responsive hADMPCs were differentiated in the absence of Dox (Dox(−)) or in the presence of 1 μg/mL Dox (Dox(+)) as described in the material and methods section. (E–I) Confirmation of differentiated cells by oil red O staining for adipocytes (E), alizarin red staining for osteocytes (F), immunohistochemical staining against collagen II for chondrocytes (G), and immunohistochemical staining against β3-tubulin for neuronal cells (H). The percentages of differentiated cells to each cell type were calculated by the computerized image analysis (I). Cells that were not induced to differentiate (non-induced) were used as a negative control. CMV; hADMPCs transduced with pTRE-EGFP-CMV-tTA-2A-Bsd, EF; hADMPCs transduced with pTRE-EGFP-EF-tTA-2A-Bsd. Scale bar, 50 μm.*
doi:10.1371/journal.pone.0066274.g005

requiring sustained, long-term expression of therapeutic proteins. In this study, we generated novel lentiviral vectors with a tet-off system, and demonstrated that our lentiviral vector systems were significantly effective and strictly regulated in hADMPCs, without affecting their stem cell properties.

Gene silencing is of considerable importance where stable, long-term expression is required. Researchers have reported that transgene silencing occurred when the CMV promoter was used in some cell types, especially in embryonic stem cells [15–17]. Since Kawabata et al. also demonstrated that virus-derived promoters inefficiently functioned in embryonic stem cells in gene transfer experiments [37], down-regulation and unsuitability of promoters in stem cells should be considered. Therefore, transduction efficacy and durability of transgene expression in hADMPCs is also an important issue to be determined. Qin et al. reported that the human EF-1α promoter and the TRE promoter are more efficient than the CMV promoter to drive lentiviral mediated transgene expression in rat bone marrow-derived MSCs [18]. McGinley et al. also showed that EF-1α and human phosphoglycerate kinase-1 (PGK) promoters have a clear advantage over the CMV promoter in transducing rat bone marrow-derived MSC transduction with lentivirus [19]. Consistent with their findings, our data also demonstrated that the EF-1α promoter was more efficient than the CMV promoter to drive EGFP expression in hADMPCs (Figure 1A, B). Moreover, a significant decrease in fluorescent intensity was observed by 28 days after transduction with lentiviral vector CSII-CMV-EGFP (Figure 1C), suggesting that the CMV promoter might be silenced in hADMPCs. We also demonstrated the intriguing finding that most (>90%) of the hADMPCs transduced with pTRE-EGFP-EF-tTA-2A-Bsd strongly expressed EGFP in the absence of Dox, whereas >50% of the cells transduced with pTRE-EGFP-CMV-tTA-2A-Bsd were EGFP negative, regardless of their blasticidin resistance (Figure 3A, B). Our data demonstrated that the inhibitor of histone deacetylation trichostatin A (TSA) re-induced the expression of EGFP (Figure 3C, D), suggesting that "promoter suppression" might occur by histone deacetylation, not by DNA methylation of CpG sites within the TRE tight promoter. "Promoter suppression" is a transcript repression of a 5′ transcriptional unit by a 3′ unit when 2 transcriptional units lie adjacent in head-to-tail tandem on a chromosome [28,29]. In this study, it is possible that the downstream unit of CMV-tTA-2A-Bsd repressed the upstream unit of TRE-EGFP because (1) resistance to blasticidin implies the transcriptional unit of CMV-tTA-2A-Bsd is active, and (2) reactivation of EGFP expression by TSA implies the transcriptional unit of TRE-EGFP is epigenetically silenced. In order to eliminate the promoter suppression or transcriptional interference between 2 transcriptional units, some researchers have been trying to separate the 2 units by polyadenylation, terminator, and insulator sequences [28,38]. However, these sequences extend the lentiviral vector size, which may affect the lentiviral titers produced from the vector. From this point of view, our finding that the transcriptional unit driven from the TRE tight promoter is resistant to gene silencing when arranged in tandem with the EF-tTA-2A-Bsd transcriptional unit (Figure 3) is of interest in the fields of both basic and clinical research, although the underlying mechanism remains elusive.

In general, large numbers of cells displaying the appropriate phenotypes are required for tissue engineering. Moreover, fully differentiated cells do not proliferate [39]. Therefore, in order to obtain enough cells to perform a transplant from genetically modified MSCs, it is important to develop a system in which the gene of interest is tightly regulated and inducible, and in which stably expressing transgenic cell lines can be obtained without affecting their stem cell properties. Using the system, MSCs transduced with lentiviral vectors can be selected and increased in numbers from a limited number of MSCs, before the target genes are induced. After obtaining an adequate number of gene-manipulated MSCs, the target genes could be induced in order to start differentiation. According to our data, hADMPCs transduced with pTRE-EGFP-EF-tTA-2A-Bsd were successfully selected by blasticidin, could proliferate, maintain their stem cell properties, and regulate EGFP expression tightly by Dox (Figure 4, 5), demonstrating that this all-in-one lentiviral vector is a promising gene delivery system for generating the material for artificial organs.

A major advantage of using the 2A cleavage factor in the construction of multi-cistronic vectors is its small size compared to internal promoter entry site (IRES) sequences. Because the titer of the lentivirus decreases with increasing size of the lentiviral vector, it is important to minimize the length of the sequences. In addition, linkage of 2 genes by 2A peptide resulted in efficient co-expression of the genes, whereas a gene placed downstream of an IRES is expressed at 2- to 3-fold lower levels than a gene placed upstream [40,41]. In this study, tTA-2A-Bsd cassette driven from CMV or EF-1α promoter showed ~90% cleavage (Figure 3). However, the point that should be considered is the effect of residual 2A peptide on the protein. As the processing occurred at the end of the 2A peptide, the 2A tag remains attached at the tTA C-terminus. Our data demonstrated that the presence of this extra 2A peptide did not seem to interfere with the activity of tTA since Dox strictly regulated the expression of EGFP under the control of TRE-tight promoter (Figure 2D, 3A, 3B and 5). Moreover, when Bsd is cleaved, an additional proline is attached at the N-terminus. We demonstrated that this did not affect a function of Bsd because hADMPCs transduced with either pTRE-EGFP-CMV-tTA-2A-Bsd or pTRE-EGFP-EF-tTA-2A-Bsd could survive and proliferate in medium containing blasticidin at a concentration at which all of the parental hADMPCs died.

Another advantage of our lentiviral system is the availability of a restriction enzyme treatment/ligation independent cloning system, called the Gateway system (Invitrogen). In general, the construction of lentiviral vectors using a conventional restriction enzyme/ligation cloning method has poor efficiency due to the large sizes and the lack of proper cloning sites. In our hands, cloning efficiency into our new lentiviral vectors pTRE-RfA-CMV-tTA-2A-Bsd or pTRE-RfA-EF-tTA-2A-Bsd using LR recombination reaches nearly 100%, saving time and effort in construction of the vectors. In addition, there are several resources available that take advantage of the Gateway vector. For example, CCSB Human ORFeome Collection (Dana-Farber Cancer Institute, Center for Cancer Systems Biology) represents almost 12,000 fully-sequenced cloned human ORFs which can be readily transferred to Gateway compatible destination vectors for various functional proteomics studies [42]. Block-iT pol II miR RNAi system from Invitrogen, which is designed to express artificial miRNAs, also enables compatibility with Gateway destination vectors for gene knock-down experiments [43].

In conclusion, our new single tet-off lentiviral vector system provides powerful tools not only for applied research on hADMPCs and other stem cells, but also basic research on a variety of cell lines and primary cells.

Acknowledgments

We thank J. Uda, S. Tamura, C. Sone, K. Nakagita, and H. Isshi for technical support. We thank Dr. Tyler Jacks for providing the pSico plasmid and Dr. Hiroyuki Miyoshi for the CSII-EF-RfA, CSII-CMV-RfA, pCMV-VSVG-RSV-Rev, and pCAG-HIVg/p plasmids.

Author Contributions

Conceived and designed the experiments: HM MM. Performed the experiments: HM MM KS HO AM. Analyzed the data: HM MM KS. Contributed reagents/materials/analysis tools: HM MM HO AI AM. Wrote the paper: HM MM TH.

References

1. Okura H, Komoda H, Saga A, Kakuta-Yamamoto A, Hamada Y, et al. (2010) Properties of hepatocyte-like cell clusters from human adipose tissue-derived mesenchymal stem cells. Tissue engineering Part C, Methods 16: 761–770.
2. Okura H, Matsuyama A, Lee CM, Saga A, Kakuta-Yamamoto A, et al. (2010) Cardiomyoblast-like cells differentiated from human adipose tissue-derived mesenchymal stem cells improve left ventricular dysfunction and survival in a rat myocardial infarction model. Tissue engineering Part C, Methods 16: 417–425.
3. Okura H, Komoda H, Fumimoto Y, Lee CM, Nishida T, et al. (2009) Transdifferentiation of human adipose tissue-derived stromal cells into insulin-producing clusters. Journal of artificial organs : the official journal of the Japanese Society for Artificial Organs 12: 123–130.
4. Safford KM, Safford SD, Gimble JM, Shetty AK, Rice HE (2004) Characterization of neuronal/glial differentiation of murine adipose-derived adult stromal cells. Experimental neurology 187: 319–328.
5. Leu S, Lin YC, Yuen CM, Yen CH, Kao YH, et al. (2010) Adipose-derived mesenchymal stem cells markedly attenuate brain infarct size and improve neurological function in rats. Journal of translational medicine 8: 63.
6. Ikegame Y, Yamashita K, Hayashi S, Mizuno H, Tawada M, et al. (2011) Comparison of mesenchymal stem cells from adipose tissue and bone marrow for ischemic stroke therapy. Cytotherapy 13: 675–685.
7. Tan B, Luan Z, Wei X, He Y, Wei G, et al. (2011) AMP-activated kinase mediates adipose stem cell-stimulated neuritogenesis of PC12 cells. Neuroscience 181: 40–47.
8. Reid AJ, Sun M, Wiberg M, Downes S, Terenghi G, et al. (2011) Nerve repair with adipose-derived stem cells protects dorsal root ganglia neurons from apoptosis. Neuroscience.
9. Rehman J, Traktuev D, Li J, Merfeld-Clauss S, Temm-Grove CJ, et al. (2004) Secretion of angiogenic and antiapoptotic factors by human adipose stromal cells. Circulation 109: 1292–1298.
10. Lee EY, Xia Y, Kim WS, Kim MH, Kim TH, et al. (2009) Hypoxia-enhanced wound-healing function of adipose-derived stem cells: increase in stem cell proliferation and up-regulation of VEGF and bFGF. Wound repair and regeneration : official publication of the Wound Healing Society [and] the European Tissue Repair Society 17: 540–547.
11. Moriyama M, Moriyama H, Ueda A, Nishibata Y, Okura H, et al. (2012) Human adipose tissue-derived multilineage progenitor cells exposed to oxidative stress induce neurite outgrowth in PC12 cells through p38 MAPK signaling. BMC Cell Biol 13: 21.
12. Wu H, Ye Z, Mahato RI (2011) Genetically modified mesenchymal stem cells for improved islet transplantation. Mol Pharm 8: 1458–1470.
13. Pfeifer A, Ikawa M, Dayn Y, Verma IM (2002) Transgenesis by lentiviral vectors: lack of gene silencing in mammalian embryonic stem cells and preimplantation embryos. Proc Natl Acad Sci U S A 99: 2140–2145.
14. Duan HF, Wu CT, Wu DL, Lu Y, Liu HJ, et al. (2003) Treatment of myocardial ischemia with bone marrow-derived mesenchymal stem cells overexpressing hepatocyte growth factor. Mol Ther 8: 467–474.
15. Brooks AR, Harkins RN, Wang P, Qian HS, Liu P, et al. (2004) Transcriptional silencing is associated with extensive methylation of the CMV promoter following adenoviral gene delivery to muscle. J Gene Med 6: 395–404.
16. Kim S, Kim GJ, Miyoshi H, Moon SH, Ahn SE, et al. (2007) Efficiency of the elongation factor-1alpha promoter in mammalian embryonic stem cells using lentiviral gene delivery systems. Stem Cells Dev 16: 537–545.
17. Meilinger D, Fellinger K, Bultmann S, Rothbauer U, Bonapace IM, et al. (2009) Np95 interacts with de novo DNA methyltransferases, Dnmt3a and Dnmt3b, and mediates epigenetic silencing of the viral CMV promoter in embryonic stem cells. EMBO Rep 10: 1259–1264.
18. Qin JY, Zhang L, Clift KL, Hulur I, Xiang AP, et al. (2010) Systematic comparison of constitutive promoters and the doxycycline-inducible promoter. PLoS One 5: e10611.
19. McGinley L, McMahon J, Strappe P, Barry F, Murphy M, et al. (2011) Lentiviral vector mediated modification of mesenchymal stem cells & enhanced survival in an in vitro model of ischaemia. Stem Cell Res Ther 2: 12.
20. Weber W, Fussenegger M (2006) Pharmacologic transgene control systems for gene therapy. J Gene Med 8: 535–556.
21. Shi Q, Tian X, Zhao Y, Luo H, Tian Y, et al. (2011) Anti-arthritic effects of FasL gene transferred intra-articularly by an inducible lentiviral vector containing improved tet-on system. Rheumatol Int.
22. Wiederschain D, Wee S, Chen L, Loo A, Yang G, et al. (2009) Single-vector inducible lentiviral RNAi system for oncology target validation. Cell Cycle 8: 498–504.
23. Hioki H, Kuramoto E, Konno M, Kameda H, Takahashi Y, et al. (2009) High-level transgene expression in neurons by lentivirus with Tet-Off system. Neurosci Res 63: 149–154.
24. Benabdellah K, Cobo M, Munoz P, Toscano MG, Martin F (2011) Development of an all-in-one lentiviral vector system based on the original TetR for the easy generation of Tet-ON cell lines. PLoS One 6: e23734.
25. Okura H, Saga A, Fumimoto Y, Soeda M, Moriyama M, et al. (2011) Transplantation of human adipose tissue-derived multilineage progenitor cells reduces serum cholesterol in hyperlipidemic Watanabe rabbits. Tissue engineering Part C, Methods 17: 145–154.
26. Saga A, Okura H, Soeda M, Tani J, Fumimoto Y, et al. (2011) HMG-CoA reductase inhibitor augments the serum total cholesterol-lowering effect of human adipose tissue-derived multilineage progenitor cells in hyperlipidemic homozygous Watanabe rabbits. Biochemical and biophysical research communications 412: 50–54.
27. Okura H, Saga A, Fumimoto Y, Soeda M, Moriyama M, et al. (2011) Transplantation of human adipose tissue-derived multilineage progenitor cells reduces serum cholesterol in hyperlipidemic Watanabe rabbits. Tissue Eng Part C Methods 17: 145–154.
28. Villemure JF, Savard N, Belmaaza A (2001) Promoter suppression in cultured mammalian cells can be blocked by the chicken beta-globin chromatin insulator 5'HS4 and matrix/scaffold attachment regions. J Mol Biol 312: 963–974.
29. Emerman M, Temin HM (1986) Comparison of promoter suppression in avian and murine retrovirus vectors. Nucleic Acids Res 14: 9381–9396.
30. Tai K, Pelled G, Sheyn D, Bershteyn A, Han L, et al. (2008) Nanobiomechanics of repair bone regenerated by genetically modified mesenchymal stem cells. Tissue Eng Part A 14: 1709–1720.
31. Goudenege S, Pisani DF, Wdziekonski B, Di Santo JP, Bagnis C, et al. (2009) Enhancement of myogenic and muscle repair capacities of human adipose-derived stem cells with forced expression of MyoD. Mol Ther 17: 1064–1072.
32. Li Y, Zhang R, Qiao H, Zhang H, Wang Y, et al. (2007) Generation of insulin-producing cells from PDX-1 gene-modified human mesenchymal stem cells. J Cell Physiol 211: 36–44.
33. Karnieli O, Izhar-Prato Y, Bulvik S, Efrat S (2007) Generation of insulin-producing cells from human bone marrow mesenchymal stem cells by genetic manipulation. Stem Cells 25: 2837–2844.
34. Dezawa M, Kanno H, Hoshino M, Cho H, Matsumoto N, et al. (2004) Specific induction of neuronal cells from bone marrow stromal cells and application for autologous transplantation. J Clin Invest 113: 1701–1710.
35. Fan L, Lin C, Zhuo S, Chen L, Liu N, et al. (2009) Transplantation with survivin-engineered mesenchymal stem cells results in better prognosis in a rat model of myocardial infarction. Eur J Heart Fail 11: 1023–1030.
36. Ghosh SS, Gopinath P, Ramesh A (2006) Adenoviral vectors: a promising tool for gene therapy. Appl Biochem Biotechnol 133: 9–29.
37. Kawabata K, Sakurai F, Yamaguchi T, Hayakawa T, Mizuguchi H (2005) Efficient gene transfer into mouse embryonic stem cells with adenovirus vectors. Mol Ther 12: 547–554.
38. Tian J, Andreadis ST (2009) Independent and high-level dual-gene expression in adult stem-progenitor cells from a single lentiviral vector. Gene Ther 16: 874–884.
39. Clarke MF, Fuller M (2006) Stem cells and cancer: two faces of eve. Cell 124: 1111–1115.
40. Chinnasamy D, Milsom MD, Shaffer J, Neuenfeldt J, Shaaban AF, et al. (2006) Multicistronic lentiviral vectors containing the FMDV 2A cleavage factor demonstrate robust expression of encoded genes at limiting MOI. Virol J 3: 14.
41. Ibrahimi A, Vande Velde G, Reumers V, Toelen J, Thiry I, et al. (2009) Highly efficient multicistronic lentiviral vectors with peptide 2A sequences. Hum Gene Ther 20: 845–860.
42. Temple G, Gerhard DS, Rasooly R, Feingold EA, Good PJ, et al. (2009) The completion of the Mammalian Gene Collection (MGC). Genome Res 19: 2324–2333.
43. Liang Z, Wu H, Reddy S, Zhu A, Wang S, et al. (2007) Blockade of invasion and metastasis of breast cancer cells via targeting CXCR4 with an artificial microRNA. Biochem Biophys Res Commun 363: 542–546.

TISSUE ENGINEERING: Part A
Volume 20, Numbers 3 and 4, 2014

DOI: 10.1089/ten.tea.2012.0534

Addition of Mesenchymal Stem Cells Enhances the Therapeutic Effects of Skeletal Myoblast Cell-Sheet Transplantation in a Rat Ischemic Cardiomyopathy Model

Yasuhiro Shudo, MD,[1] Shigeru Miyagawa, MD, PhD,[1] Hanayuki Ohkura, PhD,[1,2] Satsuki Fukushima, MD, PhD,[1] Atsuhiro Saito, PhD,[1] Motoko Shiozaki, PhD,[1] Naomasa Kawaguchi, PhD,[3] Nariaki Matsuura, MD, PhD,[3] Tatsuya Shimizu, MD, PhD,[4] Teruo Okano, PhD,[4] Akifumi Matsuyama, MD, PhD,[2] and Yoshiki Sawa, MD, PhD[1]

Introduction: Functional skeletal myoblasts (SMBs) are transplanted into the heart effectively and safely as cell sheets, which induce functional recovery in myocardial infarction (MI) patients without lethal arrhythmia. However, their therapeutic effect is limited by ischemia. Mesenchymal stem cells (MSCs) have prosurvival/proliferation and antiapoptotic effects on co-cultured cells *in vitro*. We hypothesized that adding MSCs to the SMB cell sheets might enhance SMB survival post-transplantation and improve their therapeutic effects.
Methods and Results: Cell sheets of primary SMBs of male Lewis rats (r-SMBs), primary MSCs of human female fat tissues (h-MSCs), and their co-cultures were generated using temperature-responsive dishes. The levels of candidate paracrine factors, rat hepatocyte growth factor and vascular endothelial growth factor, *in vitro* were significantly greater in the h-MSC/r-SMB co-cultures than in those containing r-SMBs only, by real-time PCR and enzyme-linked immunosorbent assay (ELISA). MI was generated by left-coronary artery occlusion in female athymic nude rats. Two weeks later, co-cultured r-SMB or h-MSC cell sheets were implanted or no treatment was performed ($n = 10$ each). Eight weeks later, systolic and diastolic function parameters were improved in all three treatment groups compared to no treatment, with the greatest improvement in the co-cultured cell sheet transplantation group. Consistent results were found for capillary density, collagen accumulation, myocyte hypertrophy, Akt-signaling, STAT3 signaling, and survival of transplanted cells of rat origin, and were related to poly (ADP-ribose) polymerase-dependent signal transduction.
Conclusions: Adding MSCs to SMB cell sheets enhanced the sheets' angiogenesis-related paracrine mechanics and, consequently, functional recovery in a rat MI model, suggesting a possible strategy for clinical applications.

Introduction

A RECENT LARGE-SCALE clinical trial, in which autologous skeletal myoblasts (SMBs) were directly injected into the heart by needle, reported only modest therapeutic benefits and a substantial risk of ventricular arrhythmias, due at least partly to the delivery method.[1,2] The major drawbacks of SMB delivery by needle injection are poor cell survival in the heart, leading to insufficient paracrine effects, and mechanical myocardial injury, potentially causing lethal arrhythmia.[1–3] In contrast, cell-sheet techniques, which we developed, deliver SMBs more effectively with minimal myocardial injury, enhanced paracrine effects, and consequently better cardiac function than attained by needle injection.[4–8]

The mechanism by which damaged myocardium is restored by transplanted SMB cell sheets is complex, involving many pathways.[4–8] Recent reports show beneficial effects of SMB cell-sheet transplantation in several animal experimental models and patients with heart failure, which are primarily attributed to cytokine secretion from the transplanted cell sheets (i.e., a paracrine effect).[4–9]

However, SMB cell sheets attached to the surface of the infarcted myocardium are poorly supported by the vascular

Presented at the American Heart Association, Orlando, Florida, November 12–15, 2011.
[1]Department of Cardiovascular Surgery, Osaka University Graduate School of Medicine, Suita, Japan.
[2]Laboratory for Somatic Stem Cell Therapy, Foundation of Biomedical Research and Innovation, Kobe, Japan.
[3]Department of Pathology, Osaka University Graduate School of Medicine, Suita, Japan.
[4]Institute of Advanced Biomedical Engineering and Science, Tokyo Women's Medical University, Tokyo, Japan.

network of the native myocardium, which limits the survival of the SMBs and, consequently, their therapeutic effects.[7] Thus, conventional SMB cell-sheet transplantation might be insufficient to repair severely damaged myocardium, which has poor viability. Mesenchymal stem cells (MSCs) are used as feeder cells to support the survival, proliferation, and differentiation of co-cultured stem/progenitor cells *in vitro*.[10–12] Moreover, MSCs are advantageous for cellular therapy because they are multipotent, potentially immune privileged, and expand easily *ex vivo*. MSCs also proliferate rapidly and induce angiogenesis.[13,14]

We hypothesized that adding MSCs to the SMB cell sheets *in vitro* might enhance their survival and function after transplantation, which might enhance the benefits of SMB cell-sheet transplantation therapy. Here, we investigated whether co-culturing SMBs with MSCs would enhance the SMBs' cytokine production *in vitro*. We also examined the therapeutic effects on chronic ischemic heart failure of transplanting cell sheets created from co-cultured SMBs and MSCs, compared with SMB-only and MSC-only cell sheets.

Materials and Methods

This study was approved by the Institutional Ethics Committee of the Osaka University. Humane animal care was used in compliance with the "Principles of Laboratory Animal Care" formulated by the National Society for Medical Research, and the "Guide for the Care and Use of Laboratory Animals" prepared by the Institute of Animal Resources and published by the National Institutes of Health (Publication No. 85–23, revised 1996). All procedures and evaluations, including assessments of cardiac parameters, were carried out in a blinded manner. The authors had full access to the data and take full responsibility for its integrity. All authors have read and agreed to the article as written.

Isolation of SMBs and adipose tissue-derived mesenchymal cells, and cell-sheet preparation

Primary skeletal myoblasts of rat origin (r-SMBs) were isolated from Lewis rats (3 weeks old, male; CLEA Japan, Inc.) and expanded *in vitro* as described previously[7,8]: more than 70% of the isolated cells were actin positive and 60–70% were desmin positive, as determined by flow cytometry (data not shown). To detect r-SMBs, we used GFP transgenic Lewis rats.[15] Primary human MSCs (h-MSCs) were isolated from female subcutaneous adipose tissue samples as described.[12] h-MSCs exhibit mesenchymal morphology (Fig. 1A). Cell sheets consisting of r-SMBs or h-MSCs were prepared using temperature-responsive culture dishes (UpCell®; CellSeed), as described.[12] Cell sheets containing both r-SMBs and h-MSCs were prepared by co-culturing these cells in temperature-responsive culture dishes.

Rat myocardial infarction model and cell-sheet implantation

A proximal site of the left anterior descending coronary artery (LCA) of athymic nude rats (F344/NJcl-rnu/rnu, 8-week-old, female, 120–130 g; CLEA Japan) was permanently occluded using a thoracotomy approach. The animals were then kept in temperature-controlled individual cages for 2 weeks to generate a subacute ischemic heart failure model.[7,8,12] The rats were then divided into 4 experimental groups ($n = 10$ in each) as follows: (1) transplantation of triple-layer h-MSC cell sheets (7.5×10^5 cells per sheet), (2) transplantation of triple-layer r-SMB cell sheets (3.0×10^6 cells per sheet), (3) transplantation of triple-layer co-cultured r-SMB (3.0×10^6 cells per sheet) and h-MSC (7.5×10^5 cells per sheet) sheets, and (4) no treatment (control) (Fig. 1B). Thereafter, the rats were kept in individual cages for 4 weeks.

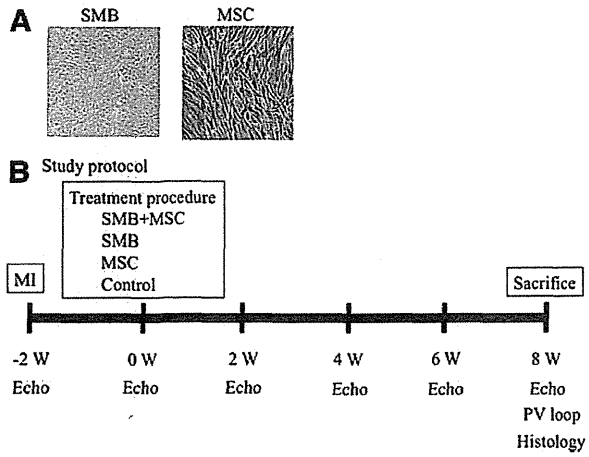

FIG. 1. **(A)** Morphology of SMB and MSC. **(B)** Study protocol used for the assessment of cardiac function and histology. Athymic nude rats (F344/NJcl-rnu/rnu) underwent induction of myocardial infarction by occluding the LAD permanently, followed by the treatment procedure 2 weeks later. Cardiac function was assessed by echocardiography just before 2, 4, 6, and 8 weeks after the treatment procedure. Eight weeks after the treatment procedure, invasive hemodynamic analysis and histological examination were performed following the sacrifice. SMB+MSC, co-culture of SMBs and MSCs; SMB, skeletal myoblast; MSC, derived mesenchymal stem cell; Echo, echocardiography; PV loop, invasive hemodynamic analysis. Color images available online at www.liebertpub.com/tea

Echocardiography

Echocardiography was performed under general anesthesia using 1% isoflurane just before, and 2, 4, 6, and 8 weeks after the treatment procedure (SONOS 7500; Philips Medical Systems) (Fig. 1B). Left ventricular end-diastolic diameter (LVEDD), left ventricular end-systolic diameter (LVESD), and end diastolic anterior wall thickness at the level of the papillary muscles were measured for at least three consecutive cardiac cycles, following the American Society for Echocardiology leading-edge method. Fractional shortening (FS) and ejection fraction (EF) were calculated as parameters of systolic function, as follows:

$$FS\ (\%) = (LVEDD - LVESD)/LVEDD$$

$$EF\ (\%) = [(LVEDD^3 - LVESD^3)/LVEDD^3].^4$$

Cardiac catheterization

To assess systolic and diastolic cardiac function, cardiac catheterization was performed under general anesthesia using 1% isoflurane, 8 weeks after the treatment procedure. A MicroTip catheter transducer (SPR-671; Millar Instruments, Inc.) and conductance catheters (Unique Medical

Co.) were placed longitudinally in the left ventricle (LV) from the apex and connected to an Integral 3-signal conditioner-processor (Unique Medical Co.). End-systolic pressure-volume relationships (ESPVR) were determined by transiently compressing the inferior vena cava. Data were recorded as a series of pressure–volume loops (~20), which were analyzed using Integral 3 software (Unique Medical Co.). The maximal and minimal rates of change in LV pressure (dP/dt max and dP/dt min, respectively) were obtained from steady-state beats using custom-made software. We assessed the early active part of the relaxation using the relaxation time constant (τ), which was determined from the LV pressure decay curve. After the hemodynamic assessment, the heart was removed for further biochemical and histological analyses.

Real-time quantitative PCR

Total RNA was extracted from cultured cell sheets or cardiac muscle tissue 8 weeks post-transplantation using TRIzol reagent (Invitrogen) and reverse transcribed into cDNA using TaqMan Reverse Transcription Reagents (Applied Biosystems). Subsequently, real-time PCR assays were performed using an ABI PRISM 7700 machine.[4,7,8] Hepatocyte growth factor (HGF), vascular endothelial growth factor (VEGF), basic fibroblast growth factor (bFGF), insulin growth factor (IGF), and thymosin β were assayed using rat-specific primers and probes (Applied Biosystems). The average copy number of gene transcripts for each sample was normalized to that for GAPDH.

Survival of grafted donor cells

The presence of grafted male cells in the female heart was quantitatively assessed by real-time PCR for the Y chromosome-specific gene *sry*. Four weeks after cell-sheet transplantation, genomic DNA was extracted from the entire LV walls using the QIAmp genomic DNA purification system (Qiagen). The signals for the autosomal single-copy gene were normalized to the amount of total DNA.[7] The primers were *sry*: forward, 5′ GCCTCAGGACATATTAATCTCTGGAG-3′; reverse, 5′-GCTGATCTCTGAATTCTGCATGC-3′.

Protein analysis

Enzyme-linked immunosorbent assay (ELISA) kits were used to measure proteins, such as HGF (Institute of Immunology) and VEGF (Quantikine; R&D) of rat origin, secreted from the cultured cell sheets *in vitro*, according to the manufacturers' suggested protocols. Values were calibrated for the extracted total proteins ($n=5$ in each group). The ELISA kits were also used to quantitatively analyze HGF (r-HGF) and VEGF (r-VEGF) of rat origin in heart tissue lysates ($n=5$ in each group).

Cytokine/chemokine multiplex immunology assay

The amount of each protein secreted from the cultured cell sheets *in vitro* was measured by Milliplex Rat Cytokine/Chemokine Panel Premixed 32Plex (Millipore), according to the manufacturer's instructions.[4] In this procedure, we applied human SMBs (h-SMBs) isolated and cultured from the patient (age 53 years, male) and expand *in vitro* as described previously.[6]

Histological analyses

Eight weeks after cell-sheet implantation, the hearts were dissected, fixed in 4% paraformaldehyde, and embedded in either optimum cutting temperature compound for 5-μm-thick cryosections or paraffin for 5-μm-thick sections ($n=5$ in each group) (Fig. 1). The paraffin-embedded sections were used for routine hematoxylin–eosin (HE) staining to assess the myocardial structure. Masson's trichrome staining was performed to assess cardiac fibrosis in the remote myocardium. The fibrotic cardiac area was calculated as the percentage of myocardial area. The data were collected from 10 individual views per heart at a magnification of ×200. The heart sections were also stained with an antibody to von Willebrand Factor (vWF) to assess capillary density, which was calculated as the number of positively stained capillary vessels that were 5–10 μm in diameter in 10 randomly selected fields in the peri-infarct area, per heart. To determine the extent of apoptosis, sections from frozen tissue samples were subjected to terminal deoxynucleotidyl transferase-mediated dUTP nick end labeling (TUNEL) with an *in situ* apoptosis detection kit (Apoptag; Chemicon). Image J software was used for quantitative morphometric analysis.

To detect r-SMBs, we used GFP transgenic Lewis rats.[15] Cryosections were stained with an anti-HGF antibody (1:50 dilution; LifeSpan BioSciences). To detect h-MSCs and differentiation of the transplanted cell sheet, sections were stained with an antibody to human leukocyte antigen (1:50 dilution; Dako). The secondary antibody was Alexa Fluor 555 goat anti-mouse (1:200 dilution; Molecular Probes). Cell nuclei were counterstained with 6-diamidino-2-phenylindole (DAPI; Invitrogen). The images were examined by fluorescence microscopy (Keyence).

Western blotting

Tissue homogenates from LV samples in the cell-sheet transplanted site ($n=3$ in each group, on day 1) were prepared using lysis buffer (100 mM Tris pH 7.4, 20% SDS, 10 mM EDTA. 10 mM NaF, 2 mM sodium orthovanadate). The equivalent total protein was loaded onto SDS-polyacrylamide gel electrophoresis gels. Antibodies obtained from Cell Signaling were antiphosphorylated STAT3 (#9145), antiphosphorylated Akt (#4051), anti-Bcl_2 (#2876), and anti-poly (ADP-ribose) polymerase (PARP) (#9542). The labeled membrane was stripped and then re-probed with anti-STAT3 (#9132), anti-AKT (#9272), and anti-cleaved PARP (#9545) antibodies. Blots were scanned, and quantitative analysis was performed using Image J software. The relative proportion of the phosphorylated STAT3 was referred to that of the STAT3. The relative proportion of the phosphorylated Akt was referred to that of the Akt. The relative proportion of the PARP, cleaved PARP, Bcl_2 was referred to that of the control group.

Statistical analysis

Continuous variables are expressed as the mean ± SD. The significance of differences was determined using a two-tailed multiple *t*-test with Bonferroni correction following repeated-measures analysis of variance for individual differences. A *p*-value less than 0.05 was considered to be statistically significant. All statistical calculations were performed using the SPSS software (version 11.0; SPSS, Inc.).

Results

Production and release of cytokines/chemokines by cell sheets

Both h-SMBs and h-MSCs, as analyzed by cytokine antibody array, released abundant angiogenic factors *in vitro*, with distance profiles (Fig. 2A). Co-cultures of h-SMBs and h-MSCs showed significantly enhanced levels of HGF, VEGF, Leptin, and PECAM-1, but not of follistatin, G-CSF, IL-8, or PDGF-BB from the h-SMBs.

The seeding ratio of 4:1 r-SMBs:h-MSCs elicited the greatest *in vitro* mRNA expression of rat HGF and VEGF by real-time PCR (Fig. 2B). The mRNA levels of SMB-derived r-HGF and r-VEGF, analyzed by real-time PCR using rat-specific primers, were significantly greater in the co-cultured cell sheets than r-SMB-only ones (Fig. 2C), whereas the mRNA levels of IGF-1, bFGF, SDF-1, and TMSB4 were essentially the same (Supplementary Fig. S1; Supplementary Data are available online at www.liebertpub.com/tea). No mRNAs for cytokines of rat origin were detected in h-MSC-only cell sheets. Rat HGF and VEGF in the culture supernatants, analyzed by ELISA with rat-specific primary antibodies, were significantly higher in the co-culture supernatants than the r-SMB-only ones, and no rat cytokines were detected in the h-MSC-only supernatants (Fig. 2D).

Cardiac functional recovery after cell-sheet transplantation

The effects of cell-sheet transplantation on cardiac function were assessed in a rat chronic ischemic heart-failure model. Two weeks after permanent occlusion of the LCA, the LV developed echocardiographic features typical of chronic ischemic heart failure, including decreased FS, EF, and anterior wall thickness, and increased end-diastolic and systolic diameter (EDD and ESD, respectively). Following myocardial

A Cytokine/Chemokine multiplex immunology assay

	SMB+MSC	SMB	MSC	Medium only
Follistatin (pg/ml)	276±35*,†	350±56†	127±8.0	3.3
G-CSF (pg/ml)	333±44*,†	487±89†	7.7±0.7	1
HGF (pg/ml)	1190±256*,†	167±28†	695±44	3.8
IL-8 (pg/ml)	805±36*,†	1079±138†	579±29	0.6
Leptin (pg/ml)	1335±690*,†	262±40	195±13	59
PDGF-BB (pg/ml)	51±11*	25±2†	51±3	3.3
PECAM-1 (pg/ml)	438±70*	239±71†	386±16	64
VEGF (pg/ml)	5673±812*,†	1402±272	2019±184	1.9

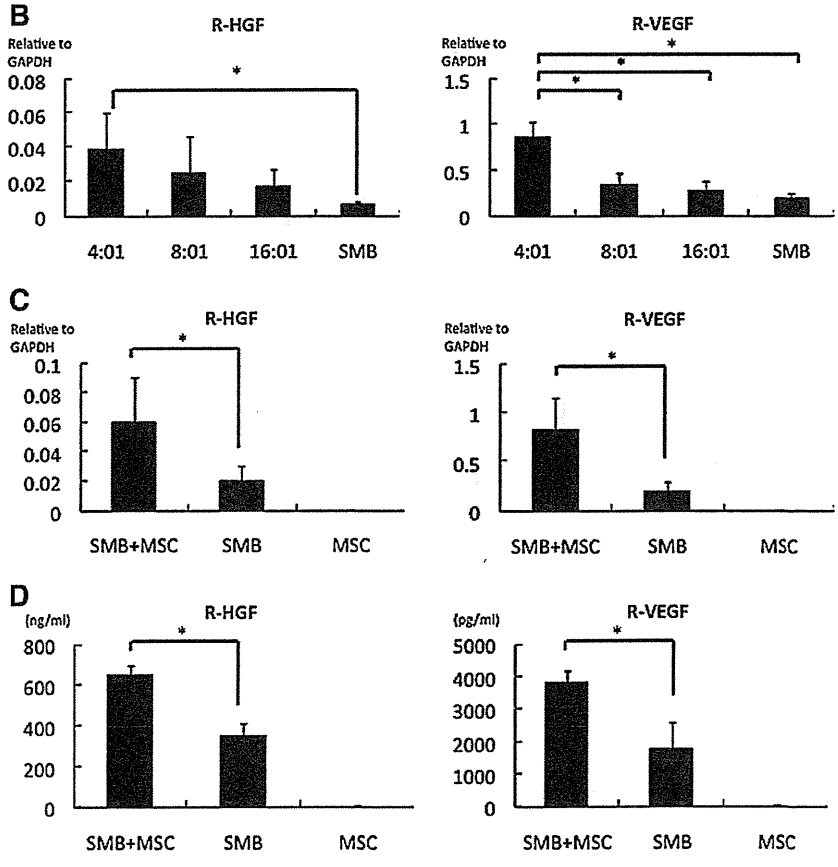

FIG. 2. Production and release of angiogenic factors by cell sheets. **(A)** Cytokine/chemokine multiplex immunology assay results from cultured cell sheets *in vitro*, prepared from human SMBs, human MSCs (h-MSCs), or both. SMB+MSC showed significantly enhanced the release of HGF, VEGF, leptin, and PECAM-1. $N=4$ in each group. $^*p<0.05$ versus SMB. $^\dagger p<0.05$ versus MSC. **(B)** Optimal seeding ratio of rat SMBs (r-SMBs) to h-MSCs. The *in vitro* mRNA levels of rat HGF and VEGF, analyzed by real-time PCR, were highest at 4:1 r-SMBs:h-MSCs. $N=4$ in each group. $^*p<0.05$. **(C)** mRNA levels in cultured cell sheets determined by real-time PCR using rat-specific primers. The SMB+MSC sheets expressed significantly more HGF and VEGF than the SMB-only ones. $N=5$ in each group. $^*p<0.05$. **(D)** Secretion of cytokines into the culture medium determined by enzyme-linked immunosorbent assay (ELISA) kits. The SMB+MSC sheets secreted significantly more HGF and VEGF than the SMB-only sheets. $N=5$ in each group. $^*p<0.05$. G-CSF, granulocyte-colony stimulating factor; HGF, hepatocyte growth factor; IL, interleukin; PDGF, platelet-derived growth factor; PECAM, platelet/endothelial cell adhesion molecule; VEGF, vascular endothelial growth factor. Error bars = SD.

infarction (MI), FS, EF, and anterior wall thickness showed steady reductions, whereas EDD/ESD showed steady increases, suggesting progressive LV remodeling.

Following either SMB-only or MSC-only cell-sheet transplantation, the heart showed mild recovery, including increases in FS, EF, and anterior wall thickness. At 2, 4, 6, and 8 weeks after treatment, FS, EF, and anterior wall thickness were significantly greater following SMB-only or MSC-only cell-sheet transplantation than the control, and significantly better recovery was obtained using the co-cultured cell sheets than either single cell-type sheet (Fig. 3A).

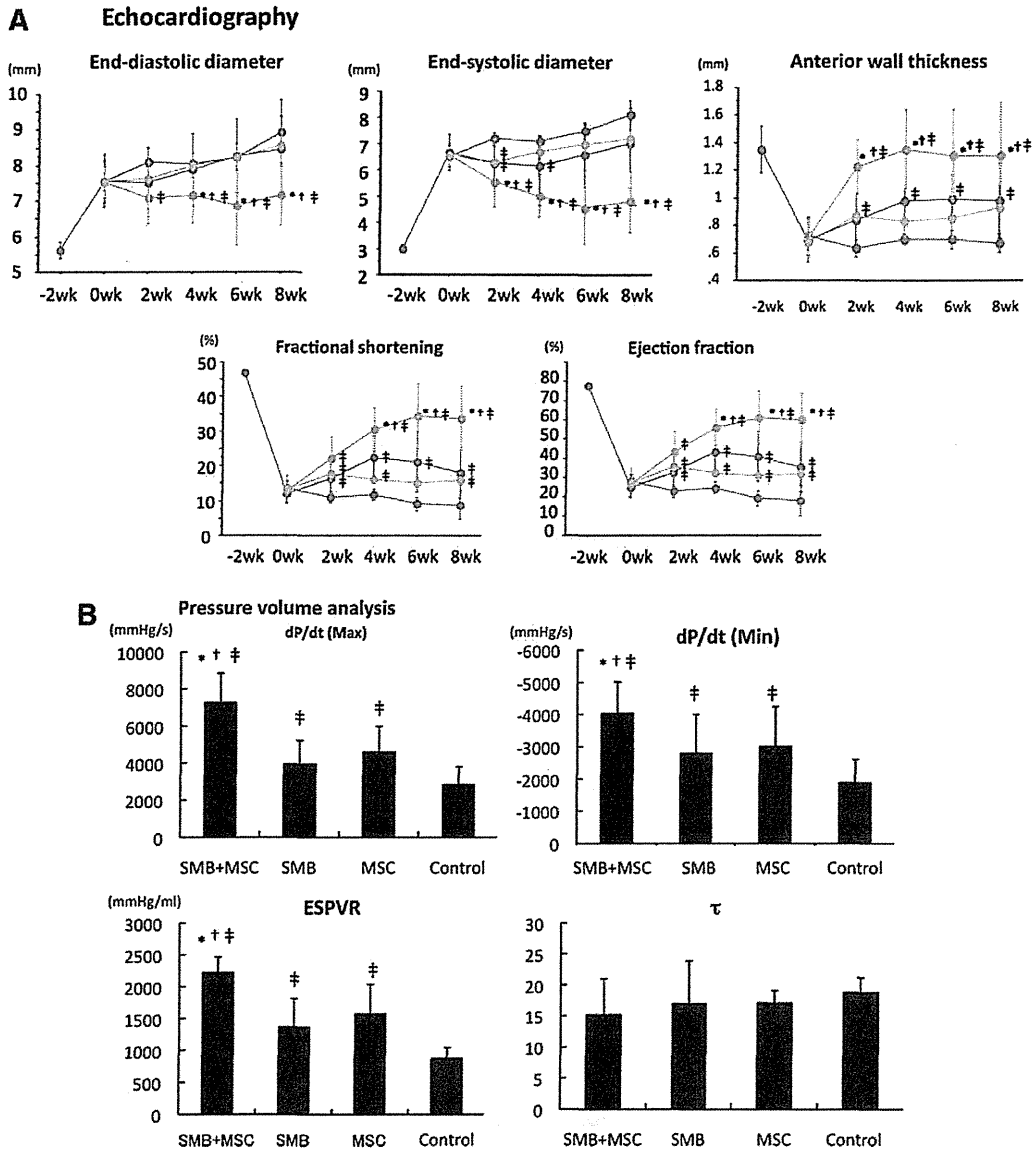

FIG. 3. Cardiac functional recovery after cell-sheet transplantation. **(A)** Echocardiographic analysis. Fractional shortening, ejection fraction, and anterior wall thickness were significantly improved 2, 4, 6, and 8 weeks after cell-sheet transplantation in the SMB+MSC sheet group, compared with the other three groups. Left ventricular end-diastolic and end-systolic diameters in the SMB+MSC sheet group were significantly decreased 4, 6, and 8 weeks after cell-sheet transplantation, compared with the other three groups ($N=10$ in each group. SMB+MSC group, green line; SMB group, blue line; MSC group, pink line; control group, red line). **(B)** Hemodynamic measurements determined by cardiac catheterization ($n=10$ in each group). Max. and min. dP/dt and ESPVR significantly improved in the SMB+MSC group, compared with the other three groups. Max. dP/dt, maximal rate of change in left ventricular pressure; min. dP/dt, minimal rate of change in left ventricular pressure; ESPVR, end-systolic pressure-volume relationship; EDPVR, end-diastolic pressure-volume relationship; τ, active part of relaxation shown by the relaxation time constant. $N=10$ in each group. $^{*}p<0.05$ versus SMB-only cell sheet. $^{\dagger}p<0.05$ versus MSC-only cell sheet. $^{\ddagger}p<0.05$ versus control. n.s., not significant. Error bars=SD. Color images available online at www.liebertpub.com/tea

Assessment by LV catheter showed a similar trend. Eight weeks after transplantation, the maximal and minimal rate of change in LV pressure (max. dP/dt and min. dP/dt, respectively) and end-systolic pressure-volume relationship (ESPVR) were significantly greater following either single-cell-type cell-sheet transplantation than the control, but τ was significantly different. After the co-culture cell-sheet transplantation, the max. dP/dt, min. dP/dt, and ESPVR improved further, with no significant difference in EDPVR or τ (Fig. 3B).

Reverse remodeling after co-culture cell-sheet transplantation

The LV structure was better maintained after SMB-only or MSC-only cell-sheet transplantation, compared to the control, in which the LV cavity was severely enlarged with a thin anterior wall, as assessed by HE staining (Fig. 4A). The LV structure was even better maintained after the co-culture cell-sheet transplantation. In the control, abundant collagen accumulations were observed in the infarct area, and diffuse fibrotic changes were induced in the remote area, whereas collagen accumulation was attenuated in both the remote area with the single cell-type sheet transplants, as assessed by Masson's trichrome staining (Fig. 4B, C). Fibrotic changes in the remote area were further attenuated by transplantation of the co-cultured cell sheet (Fig. 4D).

A greater number of vWF-positive blood vessels was detected in the peri-infarcted myocardium following the transplantation of either single-cell-type cell sheet, compared to the control (Fig. 5A), and even more vWF-positive blood vessels were seen with transplantation of the co-cultured cell sheet. The capillary density in the peri-infarcted myocardium, which was semi-quantitatively assessed in 10 randomly selected individual fields, was significantly greater following the transplantation of either single-cell-type cell sheet, compared to the control (Fig. 5B), and it was further increased after the co-cultured cell-sheet transplantation.

Major intercellular signaling molecules relevant to angiogenesis and cell survival were analyzed by western blotting. The ratio of p-STAT3 over total STAT3 was greatly increased after co-cultured cell-sheet transplantation (Fig. 5C).

Survival of transplanted cells in the heart

Four weeks after the cell-sheet transplantation, significantly more transplanted rat cells survived in co-cultured sheets than SMB-only sheets, as analyzed by PCR assays for the Y-chromosome-specific *Sry* gene (Fig. 6A).

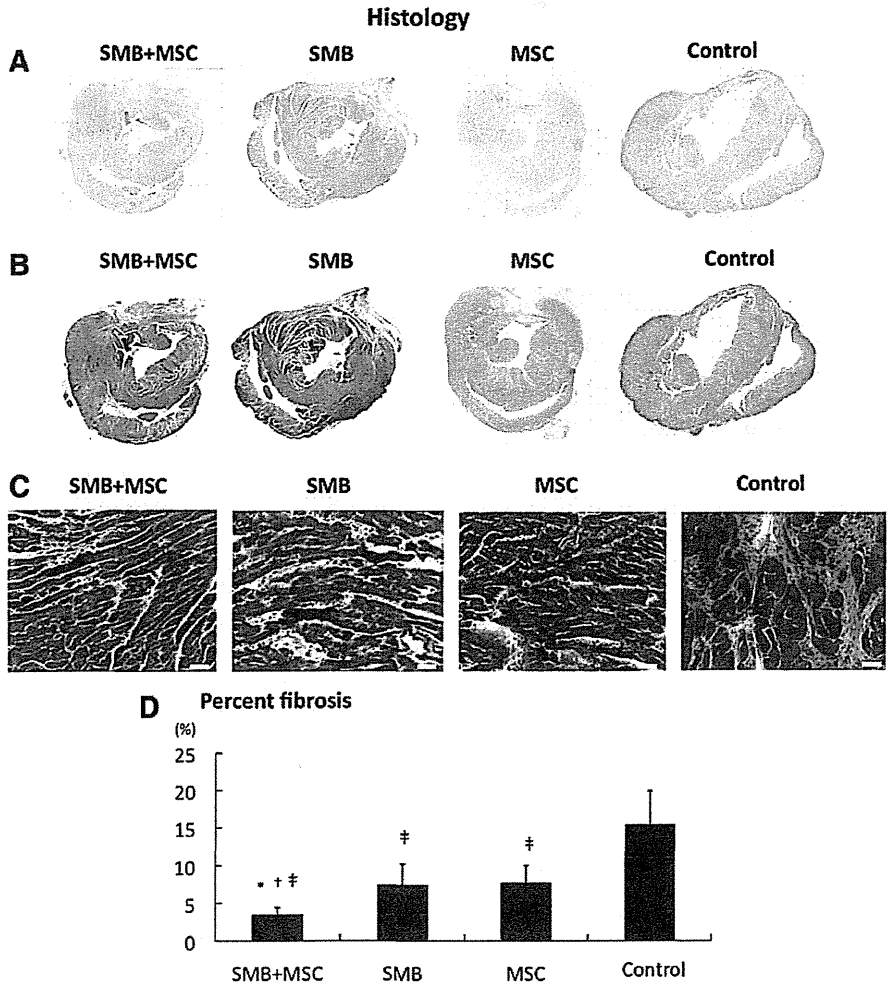

FIG. 4. Histological reverse remodeling after cell-sheet transplantation. **(A)** Macroscopic (×40) views of the heart stained by hematoxylin–eosin. **(B)** Macroscopic (×40) views of the heart stained by Masson's trichrome. **(C)** Microscopic (×200) representative Masson's trichrome staining at the remote myocardium (white bar = 40 μm). **(D)** Quantification of percent fibrosis at the remote area. Significant suppression of fibrosis was found after SMB + MSC sheet transplantation compared with the other three groups. $N = 5$ in each group. $^{*}p < 0.05$ versus SMB. $^{\dagger}p < 0.05$ versus MSC. $^{\ddagger}p < 0.05$ versus control. Error bars = SD. Color images available online at www.liebertpub.com/tea

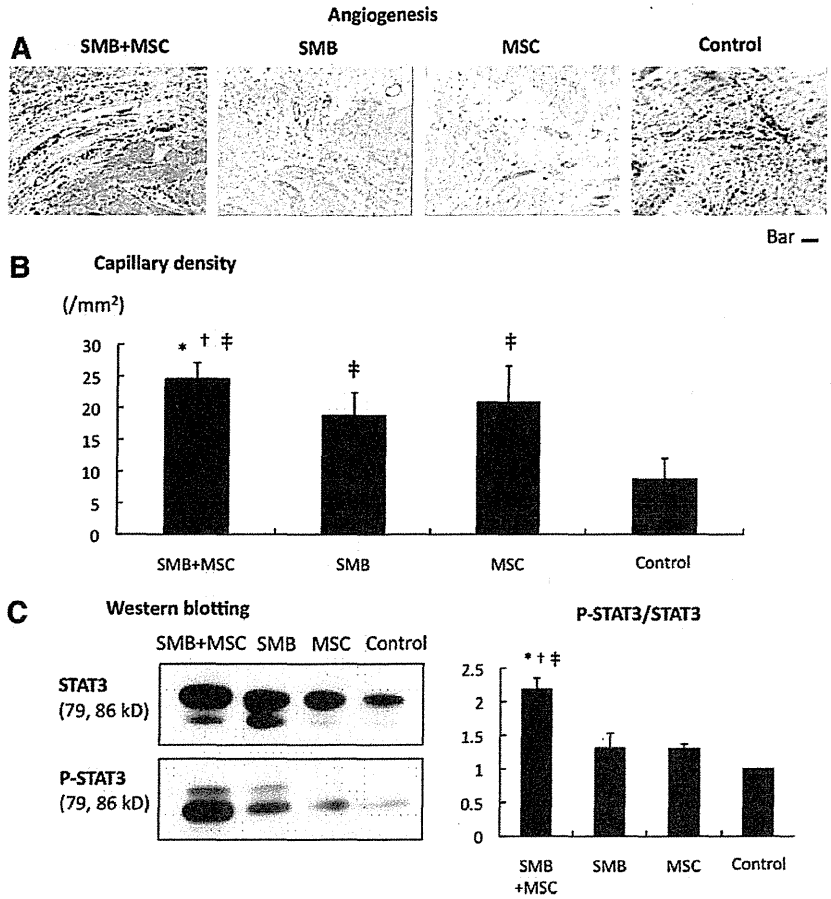

FIG. 5. Angiogenesis. **(A)** Microscopic (×100) views of sections of the peri-infarct border-zone region stained with anti-von Willebrand factor antibody (factor VIII) in the four groups (bar = 50 μm). **(B)** Capillary density: the SMB + MSC group showed significant improvement in capillary density as assessed by immunostaining for von-Willebrand factor-positive blood vessels. $N = 5$ in each group. **(C)** Western blotting showing enhanced STAT3 phosphorylation over total STAT3 in the SMB + MSC sheet group. $N = 3$ in each group. $^{*}p < 0.05$ versus SMB. $^{\dagger}p < 0.05$ versus MSC. $^{\ddagger}p < 0.05$ versus control. Error bars = SD. STAT3, signal transducer and activator of transcription 3. Color images available online at www.liebertpub.com/tea

The percentage of TUNEL-positive myocytes was significantly lower following the transplantation of the co-cultured cell sheet compared to the control (Fig. 6B).

Akt-1 and Bcl-2 were highly expressed in the heart following transplantation of the SMB-only or co-cultured cell sheet, compared with the control, as analyzed by real-time quantitative PCR using rat-specific primers (Fig. 6C).

Notably, among apoptosis-signaling molecules, Bcl_2 and cleaved PARP were increased 1 day after the co-culture cell-sheet transplantation. There was no significant difference in the ratio of phosphorylation of Akt over Akt (Fig. 6D).

Upregulation of cardioprotective factors in the myocardium after cell-sheet transplantation

The mRNA expression of cardioprotective factors, such as HGF, VEGF, IGF-1, and bFGF, in the infarct and infarct-remote areas of the myocardium was analyzed by real-time PCR using rat-specific primers, which detected factors released by transplanted SMB or the native myocardium. The expression of these factors was not significantly different after transplantation of either single-cell-type cell sheet or no treatment, except for HGF expression in the infarct area, which was significantly greater after the SMB-only sheet transplantation (Fig. 7A, B). In contrast, following transplantation of the co-cultured cell sheet, the HGF and VEGF levels in the infarct area were significantly greater than after transplantation of either single cell-type cell sheet or control, although the levels of IGF-1 and bFGF were unchanged (Fig. 2A). The intramyocardial protein levels of HGF and VEGF, analyzed by ELISA, were significantly greater after transplantation of the co-cultured cell sheet than of either single-cell-type cell sheet or no treatment (Fig. 7C).

Immunoconfocal microscopy showed that HGF was found in the transplanted SMBs from the co-cultured cell sheet (Fig. 8A).

MSCs differentiate into new vessels in situ

The differentiation capacity of the transplanted h-MSCs was assessed by immunoconfocal microscopy. As expected, no human-derived cells were seen in either the r-SMB-only transplantation group or the control group. However, human vWF-positive staining was observed in the host vessels in both the co-cultured cell-sheet group and the h-MSC-only cell-sheet transplantation group. Thus, the h-MSCs could differentiate into vessel walls *in vivo* (Fig. 8B).

Discussion

Here, we demonstrated that SMB cell sheets abundantly synthesized and extracellularly released multiple cytokines and chemokines, and adding MSCs enhanced the SMB cell

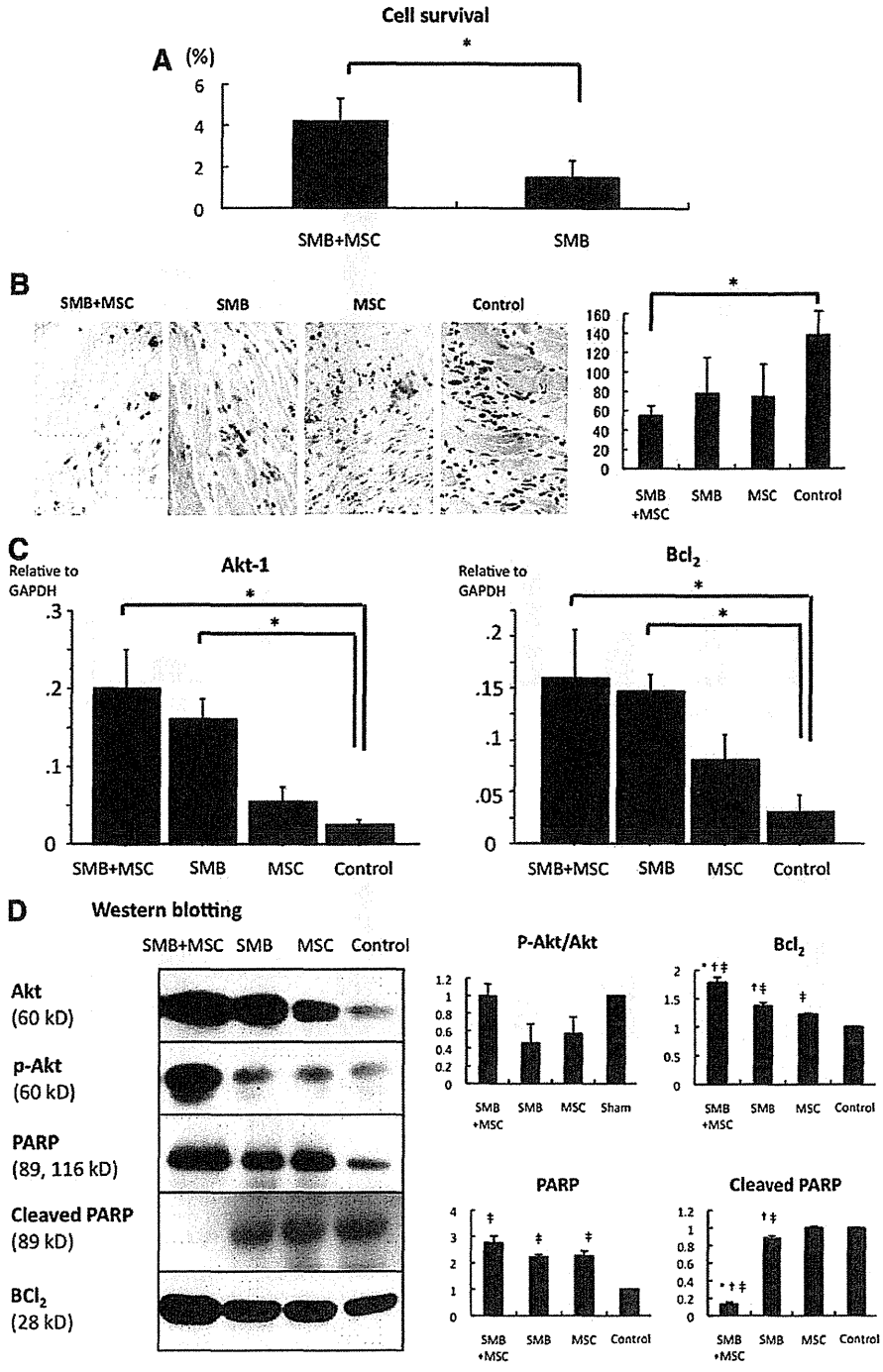

FIG. 6. Cell survival. **(A)** Survival of transplanted cells of rat origin was significantly greater in the SMB+MSC sheet group than in the SMB sheet group. $N = 4$ in each group. $^{*}p < 0.05$. **(B)** The number of terminal deoxynucleotidyl transferase-mediated dUTP nick end labeling (TUNEL)-positive myocytes was significantly lower in SMB+MSC group than in control. $N = 4$ in each group. $^{*}p < 0.05$. **(C)** Expressions of mRNA in the transplanted infarct area of hearts were determined by real-time PCR using rat-specific primers. The expressions of Akt-1 and Bcl_2 mRNA were significantly increased in the SMB+MSC sheet group compared with the other groups. $N = 4$ in each group. $^{*}p < 0.05$. **(D)** Western blotting showed that Bcl_2 was much more enhanced, and cleaved PARP was significantly downregulated in the SMB+MSC group. There was no significant difference in the ratio of phosphorylation of Akt over Akt. $N = 3$ in each group. $^{*}p < 0.05$ versus SMB. $^{\dagger}p < 0.05$ versus MSC. $^{\ddagger}p < 0.05$ versus control. Error bars = SD. Color images available online at www.liebertpub.com/tea

sheets' release of HGF and VEGF but not of IGF-1, bFGF, or SDF-1, *in vitro*. The transplantation of SMB-only cell sheets into the chronically ischemic failing rat heart resulted in reversed LV remodeling, including increased capillaries, attenuated collagen accumulation, and prolonged cell survival, which increased global functional recovery, mediated by the paracrine effects of upregulated HGF and VEGF in the myocardium.

Recent studies, including ours,[3–9] have suggested that a paracrine effect mediated by cytokines secreted from the transplanted cell sheets is a likely mechanism for the therapeutic effects on the myocardium, which was a focus of the present study. Here, we added h-MSCs to the cell sheets to enhance the potential performance of the transplanted r-SMB sheets. Our *in vitro* findings, that h-MSCs enhanced rat mRNA levels and the secretion of cytokines such as r-HGF

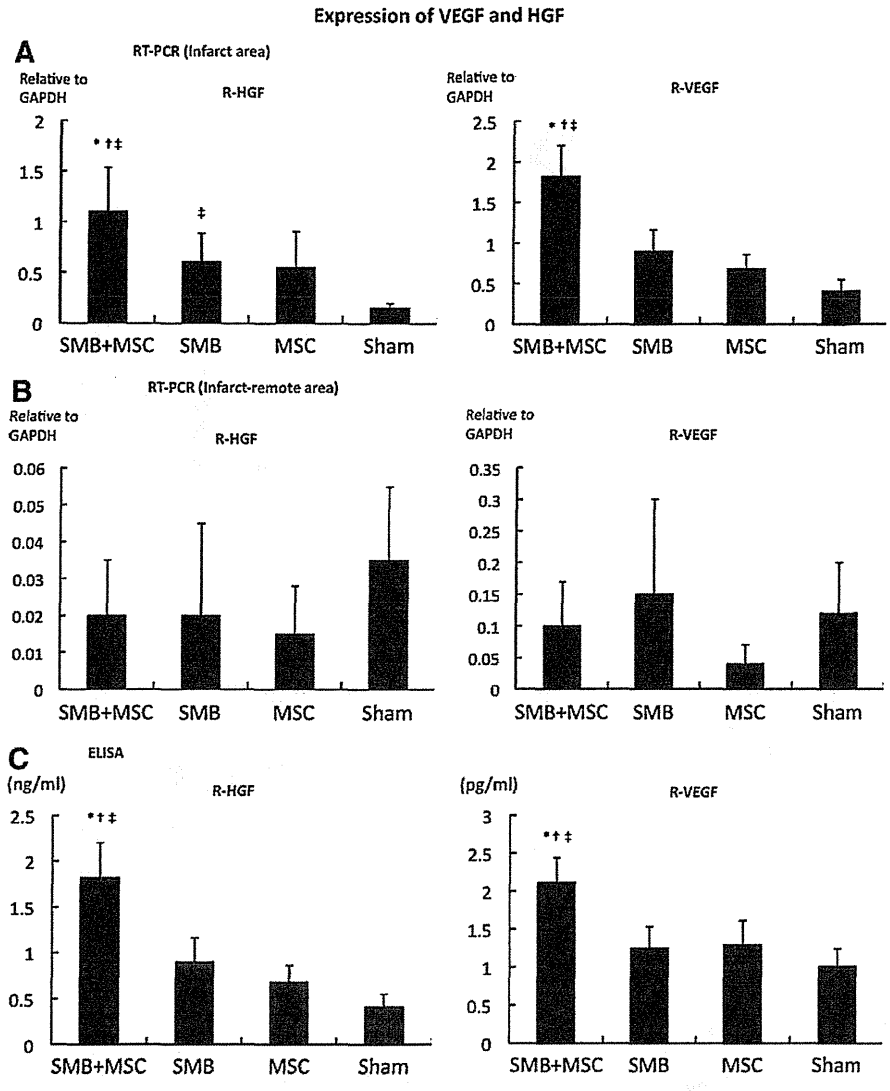

FIG. 7. Expression of VEGF and HGF is higher at the infarct area. **(A, B)** Levels of mRNA in the transplanted infarct and infarct-remote heart areas by real-time PCR using rat-specific primers. The HGF and VEGF mRNA expressions within the transplanted infarct area of the hearts were significantly increased in the SMB+MSC sheet group compared with the other groups. $N=4$ in each group. $^{*}p<0.05$ versus SMB. $^{\dagger}p<0.05$ versus MSC. $^{\ddagger}p<0.05$ versus sham. **(C)** Intramyocardial protein levels of HGF and VEGF, analyzed by ELISA, were significantly greater in the heart in the SMB+MSC sheet group compared with the other groups. $^{*}p<0.05$ versus SMB. $^{\dagger}p<0.05$ versus MSC. $^{\ddagger}p<0.05$ versus control. Error bars = SD.

and r-VEGF from r-SMBs, suggested that transplanted co-cultured cell sheets would secrete r-HGF and r-VEGF *in vivo*. Although the exact mechanisms by which "feeder layers" support cell growth have not been elucidated, it is possible that h-MSCs enhance the r-SMBs directly (via cellular interaction) or indirectly (via secreted cytokines from the h-MSCs).[16] A more comprehensive examination aimed at differentiating these effects might help reveal how feeder layers work.

HGF and VEGF participate in many complex molecular and cellular mechanisms, and their signaling pathways have been intensively investigated *in vivo*.[3,9] SMBs or MSCs act as the natural supplier of both HGF and VEGF and provide feasible and safe sources for cell therapy in clinical applications. Indeed, SMBs and bone marrow-derived mesenchymal stem cell sheets can secrete growth factors (e.g., HGF and VEGF) into the myocardium and accelerate neovascularization in the damaged area.[5–8] More recent reports have revealed that angiogenesis induced by HGF or VEGF, an antifibrotic effect promoted by HGF, or the migration and survival of SMBs supported by VEGF,[17] could be beneficial to an impaired heart.[7,8] In addition, our data from a cytokine/chemokine multiplex immunology assay indicate that leptin may also be beneficial (e.g., by inducing angiogenesis though the Jak/STAT pathway).[18] Other cytokines may also contribute to the improvement of cardiac function by single-cell-type cell sheets in as-yet-undiscovered ways.

The mechanism by which the implanted cell sheet attenuates ventricular remodeling and improves cardiac function seems to depend on the cell sheet being placed over the scarred area of the myocardium and leads to repair of the anterior wall thickness, reduction of LV wall stress, and the improvement of ejection performance.[3] Previous studies indicated that the surviving myocardium and implanted cell sheet attenuate complex cellular and molecular events, including hypertrophy, fibrosis, apoptosis of the myocardium, and the pathological accumulation of extracellular matrix.[9] Similarly, the greater cellularity observed after cell-sheet

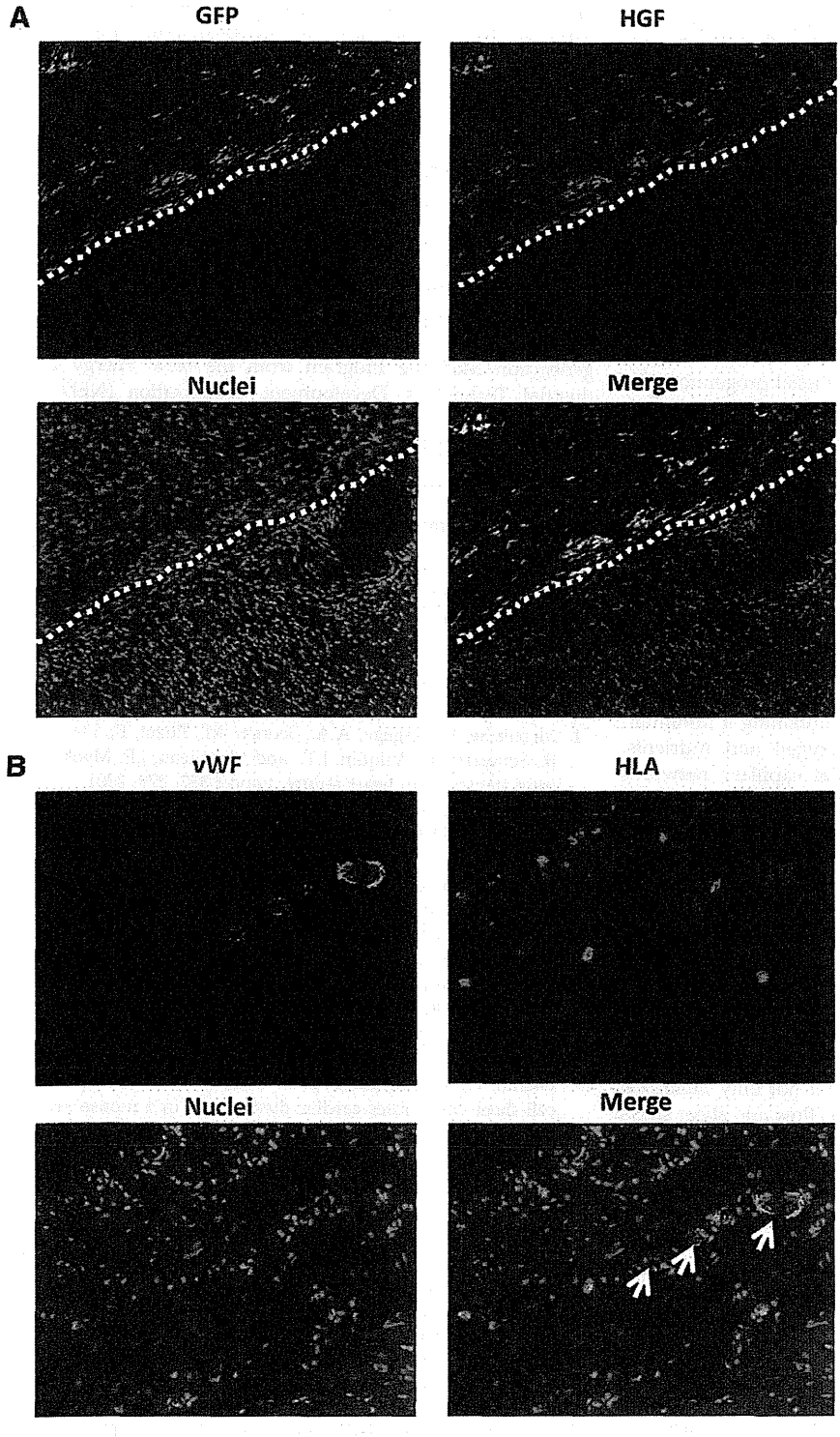

FIG. 8. Characterization of transplanted cells. **(A)** Cryosections were stained with an antibody to HGF to detect the distribution of SMB and HGF in the heart. HGF expressions and GFP-positive cells were found in the myocardium after transplantation of the SMB+MSC sheet. White broken line shows the border between the transplanted cell sheet and the host heart. Green indicates GFP; red, HGF; blue, nuclei. **(B)** Cryosections were stained with antibodies to human leukocyte antigen (HLA) and to von Willebrand factor (vWF). Human vWF-positive (white arrows) staining was observed in the host vessels in the h-MSC-transplanted group. Green indicates vWF; red, HLA; blue, nuclei. Color images available online at www.liebertpub.com/tea

treatment might have resulted from released SDF-1, which is related to cell migration, adhesion, and proliferation, by the transplanted cell sheet[19,20]

In this study, we performed additional investigations on the paracrine mechanism from a new perspective, by analyzing signaling pathways within the myocardium following cell-sheet transplantation because the signals induced by released paracrine mediators presumably activate phosphorylation cascades of signaling molecules. We found that STAT3 and Akt phosphorylations were significantly increased, and cleaved PARP was significantly downregulated, 24 h after the co-cultured cell-sheet implantation. Together

with our findings that vascular density was significantly enhanced, and myocardial apoptosis and fibrosis was significantly attenuated in the co-cultured group, it is possible that the co-cultured cell-sheet transplantation induced angiogenesis partially through the Jak/STAT signaling pathway[18] and that it prolonged cell survival by preventing apoptosis through PI-3K/Akt-mediated signaling, which is partially modulated by HGF.[21]

Although we emphasized combining SMBs with h-MSCs, some investigators have focused on different combinations of various cell sources. Sekine *et al.*[22] reported that cardiomyocytes co-cultured with endothelial cells induce greater numbers of capillaries, due to increased secretion of angiogenic growth factors.[22] Another report showed that a dermal fibroblast sheet co-cultured with endothelial progenitor cells was more effective than either single cell-type sheet for improving damaged heart function, accompanied by the inhibition of fibrotic tissue formation and the acceleration of neovascularization in the infarcted myocardium.[23] Thus, the paracrine effect may be improved by combining different cell sources; however, further investigation focused on determining the optimal combinations of cell sources is needed.

Regarding h-MSCs as a cell source, bone marrow-derived or adipose tissue-derived stem cells are reported to differentiate into mature endothelial cells and participate in blood vessel formation in the recipient heart.[24] The presence of endothelial capillary networks improves the survival and organization of implanted cells by maintaining a minimum intercapillary distance to provide oxygen and nutrients. Therefore, the presence of endothelial capillary networks may be partially correlated with cardiac function.

For future tissue engineering for cardiac therapy, the creation of thick cell-dense constructs with functional vessels may be essential. Capillary formation occurs via two basic vessel-constructing processes: angiogenesis, that is, the formation of new capillaries via sprouting or intussusception from pre-existing vessels, and vasculogenesis, which occurs in the developing embryo.[25] Here, the morphology of the vessel formation within myocardial tissues, including the diameter, composition, and fragility of vessel walls, suggested that improper vascularization may occur under pathological conditions. It is likely that not only biological factors but also physical stimuli such as flow and shear stress are required to mimic the *in vivo* environment and enable the formation of mature vascular networks.

A potential limitation of this study is that the exact number of transplanted cells was different in each group *in vivo*. Clinically, open-chest surgery is unlikely to gain easy acceptance except in certain situations; however, less invasive methods (e.g., intracoronary catheter-based procedures) might be technically difficult for carefully placing the cell sheets. Additionally, further studies that include longer timeframe than 8 weeks are needed to examine a longer term restoration of heart function post-MI. It is likely that the source of HGF is the transplanted SMB; however, it is unclear whether the source of other therapeutic cytokines is the transplanted cells, such as SMBs, MSCs, or both, or native cardiac cells.

In conclusion, we found that h-MSCs enhanced the paracrine effects of r-SMB sheets, thus enhancing angiogenesis, lowering fibrosis, inhibiting cellular hypertrophy, improving cardiac function, and prolonging cell survival in MI model rats. These observations of improved effects from this co-cultured cell sheet may lead to new regeneration therapies for heart failure following advanced cardiomyopathy that are superior to the conventional SMB-only cell-sheet technique.

Acknowledgments

We thank Dr. Eiji Kobayashi and Takashi Murakami for kindly providing the GFP transgenic Lewis rats. We thank Mr. Akima Harada, Mr. Shigeru Matsumi, and Mrs. Masako Yokoyama for their excellent technical assistance.

Sources of Funding: This study was supported by Grants for the Research and Development of the Myocardial Regeneration Medicine Program from the New Energy Industrial Technology Development Organization (NEDO), Japan. This research was supported by the Health and Labour Sciences Research Grants, Research on intractable diseases.

Disclosure Statement

T.S. is a consultant for CellSeed, Inc. T.O. is an Advisory Board Member in CellSeed, Inc., and the inventor/developer designated on the patent for temperature-responsive culture surfaces.

References

1. Menasche, P., Hagege, A.A., Scorsin, M., Puzet, B., Desnos, B., Schwartz, K., Vilquin, J.T., and Marolleau, J.P. Myoblast transplantation in heart failure. Lancet **357,** 279, 2001.
2. Hagege, A.A., Marolleau, J.P., Vilqiun, J.T., Alheritiere, A., Peyrard, S., Duboc, D., Abergel, E., Messas, E., Mousseaux, E., Schwartz, K., Desnos, M., and Menasche, P. Skeletal myoblast transplantation in ischemic heart failure: Long-term follow-up of the first phase I cohort of patients. Circulation **114,** I108, 2006.
3. Miyagawa, S., Roth, M., Saito, A., Sawa, Y., and Kostin, S. Tissue-engineered cardiac constructs for cardiac repair. Ann Thorac Surg **91,** 320, 2011.
4. Imanishi, Y., Miyagawa, S., Maeda, N., Fukushima, S., Kitagawa-Sakakida, S., Daimon, T., Hirata, A., Shimizu, T., Okano, T., Shimomura, I., and Sawa, Y. Induced adipocyte cell-sheet ameliorates cardiac dysfunction in a mouse myocardial infarction model: a novel drug delivery system for heart failure. Circulation **124,** S10, 2011.
5. Miyagawa, S., Saito, A., Sakaguchi, T., Yoshikawa, Y., Yamauchi, T., Imanishi, Y., Kawaguchi, N., Teramoto, N., Matsuura, N., Iida, H., Shimizu, T., Okano, T., and Sawa, Y. Impaired myocardium regeneration with skeletal cell sheets—a preclinical trial for tissue-engineered regeneration therapy. Transplantation **90,** 364, 2010.
6. Fujita, T., Sakaguchi, T., Miyagawa, S., Saito, A., Sekiya, N., Izutani, H., and Sawa, Y. Clinical impact of combined transplantation of autologous skeletal myoblasts and bone marrow mononuclear cells in patients with severely deteriorated ischemic cardiomyopathy. Surg Today **41,** 1029, 2011.
7. Sekiya, N., Matsumiya, G., Miyagawa, S., Saito, A., Shimizu, T., Okano, T., Kawaguchi, N., Matsuura, N., and Sawa, Y. Layered implantation of myoblast sheets attenuates adverse cardiac remodeling of the infarcted heart. J Thorac Cardiovasc Surg **138,** 985, 2009.
8. Memon, I.A., Sawa, Y., Fukushima, N., Matsumiya, G., Miyagawa, S., Taketani, S., Sakakida, S.K., Kondoh, H.,

Aleshin, A.N., Shimizu, T., Okano, T., and Matsuda, H. Repair of impaired myocardium by means of implantation of engineered autologous myoblast sheets. J Thorac Cardiovasc Surg **130,** 646, 2009.
9. Matuura, K., Honda, A., Nagai, T., Fukushima, N., Iwanaga, K., Tokunaga, M., Shimizu, T., Okano, T., Kasanuki, H., Hagiwara, N., and Komuro, I. Transplantation of cardiac progenitor cells ameliorates cardiac dysfunction after myocardial infarction in mice. J Clin Invest **119,** 2204, 2009.
10. Majumdar, M.K., Thiede, M.A., Mosca, J.D., Moorman, M., and Gerson, S.L. Phenotypic and functional comparison of cultures of marrow-derived mesenchymal stem cells (MSCs) and stromal cells. J Cell Physiol **176,** 57, 1998.
11. Richards, M., Fong, C.Y., Chan, W.K., Wong, P.C., and Bongso, A. Human feeders support prolonged undifferentiated growth of human inner cell masses and embryonic stem cells. Nat Biotechnol **20,** 933, 2002.
12. Ohkura, H., Matsuyama, A., Lee, C.M., Saga, A., Kakuta-Yamamoto, A., Nagao, A., Sougawa, N., Sekiya, N., Takekita, K., Shudo, Y., Miyagawa, S., Komoda, H., Okano, T., and Sawa, Y. Cardiomyoblast-like cells differentiated from human adipose tissue-derived mesenchymal stem cells improve left ventricular dysfunction and survival in a rat myocardial infarction model. Tissue Eng Part C Methods **16,** 417, 2010.
13. Pittenger, M.F., Mackay, A.M., Beck, S.C., Jaiswal, R.K., Douglas, R., Mosca, J.D., Moorman, M.A., Simonetti, D.W., Craig, S., and Marshak, D.R. Multilineage potential of adult human mesenchymal stem cells. Science **284,** 143, 1999.
14. Jiang, Y., Jahagirar, B.N., Reinhardt, R.L., Schwartz, R.E., Keene, C.D., Ortiz-Gonzales, X.R., Reyes, M., Lenrik, T., Lund, T., Blackstad, M., Du, J., Aldrich, S., Lisberg, A., Low, W.C., Largaespada, D.A., and Vertaille, C.M. Pluripotency of mesenchymal stem cells derived from adult marrow. Nature **418,** 41, 2002.
15. Inoue, H., Ohsawa, I., Murakami, T., Kimura, A., Hakamata, Y., Sato, Y., Kaneko, T., Takahashi, M., Okada, T., Ozawa, K., Francis, J., Leone, P., and Kobayashi, E. Development of new inbred transgenic strains of rats with LacZ or GFP. Biochem Biophys Res Commun **329,** 288, 2005.
16. Kirouac Dc, and Zandstra, P.W. Understanding cellular networks to improve hematopoietic stem cell expansion cultures. Curr Opin Biotechnol **17,** 538, 2006.
17. Germani, A., Di Carlo, A., Mangoni, A., Straino, S., Giacinti, C., Turrini, P., Biglioli, P., and Capogrosse, M.C. Vascular endothelial growth factor modulates skeletal myoblast function. Am J Pathol **163,** 1417, 2003.
18. Sierra-Honigmann, M.R., Nath, A.K., Murakami, C., García-Cardeña, G., Papapetropoulos, A., Sessa, W.C., Madge, L.A., Schechner, J.S., Schwabb, M.B., Polverini, P.J., and Flores-Riveros, J.R. Biological action of leptin as an angiogenic factor. Science **281,** 1683, 1998.
19. Hiesinger, W., Perez-Aguilar, J.M., Atluri, P., Marotta, N.A., Frederick, J.R., Fitzpatrick, J.R., 3rd, McCormick, R.C., Muenzer, J.R., Yang, E.C., Levit, R.D., Yuan, L.J., Macarthur, J.W., Saven, J.G., and Woo, Y.J. Computational protein design to reengineer stromal cell-derived factor-1a generates an effective and translatable angiogenic polypeptide analog. Circulation **124,** S18, 2011.
20. Frederick, J.R., Fitzpatrick, J.R., 3rd, McCormick, R.C., Harris, D.A., Kim, A.Y., Muenzer, J.R., Marotta, N., Smith, M.J., Cohen, J.E., Hiesinger, W., Atluri, P., and Woo, Y.J. Stromal cell-derived factor-1alpha activation of tissue-engineered endothelial progenitor cell matrix enhances ventricular function after myocardial infarction by inducing neovasculogenesis. Circulation **122,** S107, 2010.
21. Kakazu, A., Chandrasekher, G., and Bazan, H.E. HGF protects corneal epithelial cells from apoptosis by the PI-3K/Akt-1/Bad- but not the ERK 1/2-mediated signaling pathway. Invest Ophthalmol Vis Sci **45,** 3485, 2004.
22. Sekine, H., Shimizu, T., Hobo, K., Sekiya, S., Yang, J., Yamato, M., Kurosawa, H., Kobayashi, E., and Okano, T. Endothelial cell coculture within tissue-engineered cardiomyocyte sheets enhances neovascularization and improve cardiac function of ischemic hearts. Circulation **118,** S145, 2008.
23. Kobayashi, H., Shimizu, T., Yamato, M., Tono, K., Masuda, H., Asahara, T., Kasanuki, H., and Okano, T. Fibroblast sheets co-cultured with endothelial progenitor cells improve cardiac function of infarcted hearts. J Artif Organs **11,** 141, 2008.
24. Miyahara, Y., Nagaya, N., Kataoka, M., Yanagawa, B., Tanaka, K., Hao, H., Ishino, K., Ishida, H., Shimizu, T., Kangawa, K., Sano, S., Okano, T., Kitamura, S., and Mori, H. Monolayered mesenchymal stem cells repair scarred myocardium after myocardial infarction. Nat Med **12,** 459, 2006.
25. Risau, W. Mechanisms of angiogenesis. Nature **386,** 671, 1997.

Address correspondence to:
Yoshiki Sawa, MD, PhD
Department of Cardiovascular Surgery
Osaka University Graduate School of Medicine
Suita
Osaka 565-0871
Japan

E-mail: sawa-p@surg1.med.osaka-u.ac.jp

Received: September 2, 2012
Accepted: September 25, 2013
Online Publication Date: December 31, 2013